



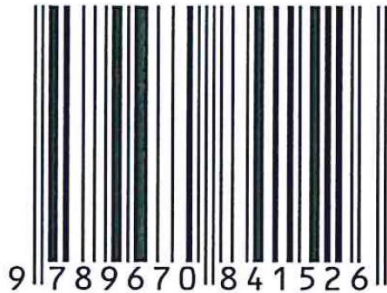
K

K O S T I

**1ST KOLOKIUUM SAINS,
TEKNOLOGI DAN
INOVASI (KOSTI)
JABATAN SAINS
GUNAAN, UITM
CAWANGAN PULAU
PINANG**

Hakmilik © 2019 oleh Jabatan Sains Gunaan, Universiti Teknologi MARA Cawangan Pulau Pinang, Penang, MALAYSIA.

eISBN 978-967-0841-52-6



Hak cipta adalah terpelihara. Tiada bahagian daripada penerbitan ini boleh diterbitkan, disimpan dalam sistem pengambilan atau dihantar dalam bentuk atau apa-apa cara, elektronik, mekanik, fotokopi, rakaman atau sebaliknya, tanpa kebenaran terlebih dahulu, secara bertulis, dari penerbit.

**JABATAN SAINS GUNAAN
UNIVERSITI TEKNOLOGI MARA CAWANGAN PULAU PINANG
PENANG, MALAYSIA**

Editor:

Ainorkhilah Mahmood (Dr.)
Mohd Haris Ridzuan Ooi Abdullah
Mohd Bukhari Md Yunus
Nor Faranaz Shamin Nor Azmi
Marina Mokhtar
Vicinisvarri Inderan
Mohd Zaki Mohd Yusoff (Dr.)
Mohd Muzafa Jumidali (Dr.)

KANDUNGAN

	MUKA SURAT
1. ENHANCING PERFORMANCE OF POROUS UNINTENTIONALLY DOPED GAN BASED MSM PHOTODETECTOR USING ALTERNATING CURRENT PHOTO-ASSISTED ELECTROCHEMICAL ETCHING (ACPEC) TECHNIQUE Amorkhilah Mahmood, Zainuriah Hassan, Alhan Farhanah Abd Rahim, Rosfariza Radzali, Naser M. Ahmed , Yushamdan Yusof	1-5
2. SOME PHYSICAL PROPERTIES OF TURKEY BERRY (<i>SOLANUM TORVUM</i>) FRUITS Mohd Haris Ridzuan Ooi Abdullah, Ch'ng Pei Eng, Mohd Firdaus Roslan	6-11
3. COGITATION OF STRUCTURAL AND MORPHOLOGY PROPERTIES OF POROUS SILICON Mohd Bukhari Md Yunus, Sharifah Nooraishah Syed Mohd Zainol, Mohd Zaki Mohd Yusoff, Muhammad Firdaus Othman	12-18
4. LITHIUM ION CAPACITOR: ELECTROCHEMICAL PROPERTIES OF PRE-DOPING ELECTRODE BY USING TOW DIFFERENT COATING TECHNIQUES Nor Faranaz Shamin Nor Azmi, Surani Buniran, Mohd Firdaus Roslee, Norha Abdul Hadi, Madhiyah Yahya, Siti Hajar Salleh, Masbudi Baharuddin	19-30
5. KAEDAH HIBRID FLIPPED CLASSROOM-PROBLEM BASED LEARNING : MENINGKATKAN KEMAHIRAN MENJAWAB SOALAN ARAS TINGGI Marina Mokhtar	31-36
6. HYDROTHERMAL SYNTHESIS OF FE DOPED TIN OXIDE (SNO₂) NANORODS FOR ETHANOL GAS SENSOR Vicinisvarri Inderan, Kumar Sudesh, Hooi Ling Lee	37-40
7. STRUCTURAL AND OPTICAL CHARACTERIZATION OF POROUS ZINC OXIDE (ZNO) GROWN ON DIFFERENT SUBSTRATES BY AMMONIUM HDYROXIDE (NH₄OH) SOLUTION Mohd Zaki Mohd Yusoff, Nur Hazwani Abu, Mohd Muzafa Jumidali, Mohd Bukhari Md Yunus, Muhammad Firdaus Othman	41-45
8. FABRICATION AND CHARACTERIZATION OF ZINC OXIDE (ZNO) THIN FILMS ON GLASS SUBSTRATE BY RADIO FREQUENCY (RF) SPUTTERING TECHNIQUE Mohd Muzafa Jumidali, Siti Amira Norafarih An Ismoni, Mohd Zaki Mohd Yusoff, Mohd Bukhari Md Yunus, Muhammad Firdaus Othman	46-50

**ENHANCING PERFORMANCE OF POROUS UNINTENTIONALLY DOPED GAN BASED
MSM PHOTODETECTOR USING ALTERNATING CURRENT PHOTO-ASSISTED
ELECTROCHEMICAL ETCHING (ACPEC) TECHNIQUE**

Ainorkhilah Mahmood^{1,a,*}, Zamuriah Hassan^{2,b}, Alhan Farhanah Abd Rahim^{3,c}, Rosfariza Radzali^{3,d}, Naser M. Ahmed^{4,e}, Yushamdan Yusof^{4,f}

¹*Department of Applied Sciences, Universiti Teknologi MARA Cawangan Pulau Pinang, 13500 Permatang Pauh, Penang, MALAYSIA.*

²*Institute of Nano Optoelectronics Research and Technology Laboratory (INOR), Universiti Sains Malaysia, 11800 Penang, MALAYSIA.*

³*Faculty of Electrical Engineering, Universiti Teknologi MARA Cawangan Pulau Pinang, 13500 Permatang Pauh, Penang, MALAYSIA.*

⁴*Nano- Optoelectronics Research and Technology Laboratory, School of Physics, Universiti Sains Malaysia, 11800 Penang, MALAYSIA.*

(E-mail: ^aainorkhilah_sp@ppinang.uitm.edu.my, ^bzai@usm.my, ^calhan570@ppinang.uitm.edu.my, ^drosfariza074@ppinang.uitm.edu.my, ^enaser@usm.my, ^fyushamdan@usm.my)

ABSTRACT - In this work, we report the formation of porous unintentionally doped (UID) n-type GaN films under a novel alternating current (sine-wave a.c. (50 Hz)) photo-assisted electrochemical etching (ACPEC) conditions. The formation of porous unintentionally doped (UID) n-type GaN by the novel ACPEC is performed in the same electrolyte concentration (4% KOH) used in common dc constant current electrochemical etching process. Ultra-violet (UV) illumination is used to assist in the generation of electron-hole pairs, where etching proceeds through the oxidation and consequently, dissolution of the semiconductor surface. The ac formed UID porous GaN with excellent structural and optical properties. According to the FESEM micrographs, the GaN thin films exhibit a homogeneous nanoarchitecture of the porous structures with perfect hexagonal shape. The porous layer exhibited a substantial photoluminescence (PL) intensity enhancement with red-shifted band-edge PL peaks associated with the relaxation of compressive stress. The shift of E₂(high) to the lower frequency in Raman spectra of the UID porous GaN films further confirms such a stress relaxation. Electrical characterizations of the MSM photodiodes were carried out by using current-voltage (I-V) measurements indicated that the devices were highly sensitive to ambient light

Keywords: Porous unintentionally doped (UID) n-type GaN; Alternating current photo-assisted electrochemical etching (ACPEC); Field Effect Scanning Electron Microscopy (FESEM); Photoluminescence; Raman spectroscopy; metal-semiconductor-metal-photodetector

1. INTRODUCTION

The interest in porous GaN has increased in recent years due to their prosperous future as the materials for fabricating the optoelectronic devices, low temperature electronic devices such as MSM photodetector and gas sensor. After the discovery of room temperature photoluminescence enhancement from porous GaN by Shelton et al. [1], the structural and optical properties of the porous GaN have been greatly investigated [2-5]. Due to its simple fabrication process, interesting optical properties, research in porous GaN has progressed in wide a range of novel

ideas and applications such as gaseous sensor [6, 7], photodetector [8] and chemical sensor [9]. Many other sensing applications based on the large, nanostructure surface area of porous GaN may be imagined. One such example is to use the porous GaN as a template for metal deposition for surface enhanced Raman (SERS) substrates [10]. Porous GaN is an excellent candidate for this application, due to it offering nanoscale features, high surface area, and large homogeneous surface. Porous GaN can be prepared through dry-etching techniques, such as ion milling, chemical-assisted ion beam etching, reactive ion etching, and inductively coupled plasma reactive ion etching. However, these methods could induce surface damage; moreover, they lack the desired selectivity for the morphology, dopant, and composition[11]. The most feasible and cost-effective method to prepare porous GaN is the direct current (DC) photo-assisted electrochemical etching. To gain a high porosity layer, the most common technique is to use DC conditions with a constant and relatively high current density. Although dramatic research has been conducted to understand the formation of porous GaN prepared by the common technique, substantial fundamental properties are still not well understood[5, 12-17]. The goal of this study is to prepare UID porous GaN by a novel technique, namely by alternating current photo-assisted electrochemical etching (ACPEC)[18]. Result of the surface morphology, optical properties and electrical characteristics of the samples are reported.

2. EXPERIMENTAL METHOD

The samples used in this study are commercial unintentionally doped (UID) n-type GaN grown by metalorganic chemical vapor deposition (MOCVD) on two-inch sapphire (0001) substrates. The thickness of the GaN film is 3 μm with carrier concentration of $\sim 6.05 \times 10^{17} \text{ cm}^{-3}$, as determined by the Hall measurements. In the AC photoelectrochemical etching process, we used an alternating current density of $J = 50 \text{ mA/cm}^2$ for 45, 90 and 120 min. The ac etching process was performed at room temperature under illumination of 500 W ultra-violet (UV) lamp in 4% concentration of KOH electrolyte. Typical electrochemical cell for the generation of UID porous GaN are schematically shown in Figure 1.

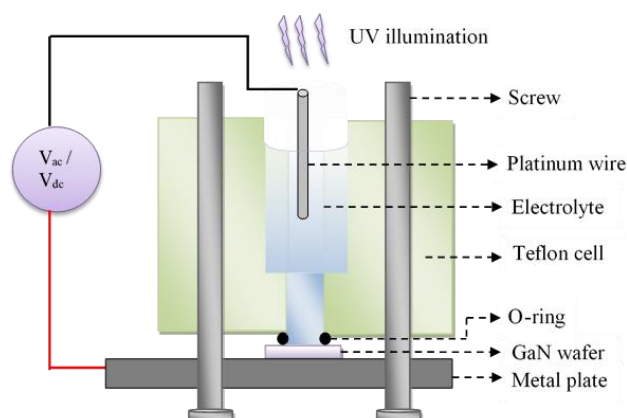


Figure 1. Schematic of alternating current photo-assisted electrochemical etching (ACPEC) apparatus.

The surface morphology and optical properties of the samples are investigated by FESEM, AFM, HR-XRD, Raman and photoluminescence spectroscopy. The electrical characteristics are extracted from MSM photodetector.

3. RESULTS AND DISCUSSION

Figure 2 shows a plan view of the sample etched with 50 mA/cm^2 . Figure 2(a) and Figure 2(b) shows that at 45 min, pores start to appear in an early development of the nanoarchitecture of the porous structure. Upon removal of the material of the grains in the top layer, subsequent etching takes place in the sub-grains at the lower layer and so on, creating novel layered nanoarchitecture of the porous structure [18, 19]. The more rapid evolution of the pore morphology is evident in Figure 2(c) for the sample etched at 90 min. At 120 min, nanoarchitecture of the porous structure are fully developed with perfect hexagonal shape. To understand these conditions, the reaction mechanism between electrolytes and GaN surface must be understood. Electron-hole pairs were generated on the surface of GaN by an incident of UV light, the reaction among Ga^+ and OH^- ions forms N_2 and Ga_2O_3 , which dissolves in the solution and forming uniform pores [4, 20]. Similar structure has been observed by Hartono et al.[21] in porous GaN. It is interesting to note, however, that the porous GaN prepared by the electrochemical etching method does not always produce similar surface morphology. For example, GaN fabricated by Yam et al.[22] was covered with star, elongated, triangular and squarish type of pores.

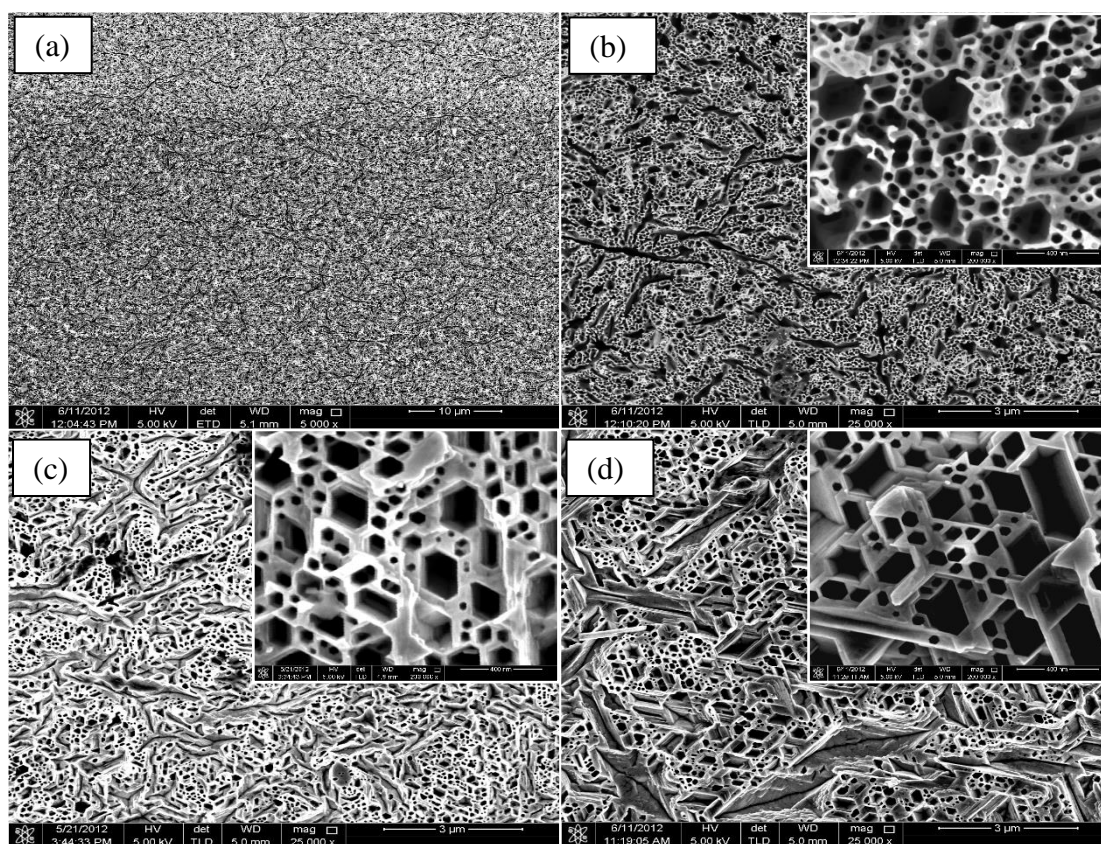


Figure 2. FESEM image of the unintentionally doped porous GaN formed under different etching duration with a current density of $ac \ 50 \text{ mA/cm}^2$ (a) 45 minutes at 5K magnification (b) 45 minutes (c) 90 minutes, and (d) 120 minutes. Inset is the image with higher magnification.

4. CONCLUSION

In summary, a novel, simple and cost-effective alternating current PEC etching was demonstrated to be an effective technique for the formation of nano-porous GaN with excellent properties. According to FESEM images, the etching duration has significant impact on the size of the pores. AFM measurements evidenced that surface roughness increased in porous samples. The obtained results hint at the possibility to prepare high quality nano-porous GaN layers with

tuneable stress. We strongly believe that further refinements of the sine-wave ac electrochemical processing technologies will enhance their role in semiconductor nanotechnology and nanoelectronics in the near future.

5. REFERENCES

1. Shelton, B.S., et al., *Ultrasooth GaN Etched Surfaces Using Photoelectrochemical Wet Etching and an Ultrasonic Treatment*. Electrochemical and Solid-State Letters, 2000. **3**(2): p. 87-89.
2. Vajpeyi, A.P., et al., *Investigation of optical properties of nanoporous GaN films*. Physica E: Low-dimensional Systems and Nanostructures, 2005. **28**(2): p. 141-149.
3. Chuah, L.S., et al., *Surface Morphology and Formation of Nanostructured Porous GaN by UV-assisted Electrochemical Etching*. World Academy of Science, Engineering and Technology 2009. **55**: p. 16.
4. Al-Heuseen, K., M.R. Hashim, and N.K. Ali, *Effect of different electrolytes on porous GaN using photo-electrochemical etching*. Applied Surface Science, 2011. **257**(14): p. 6197-6201.
5. Mahmood, A., et al., *Structural and Surface Studies of Undoped Porous GaN Grown on Sapphire*. Advanced Materials Research, 2013. **620**: p. 45-49.
6. Al-Heuseen, K. and M.R. Hashim, *Enhancing hydrogen sensitivity of porous GaN by using simple and low cost photoelectrochemical etching techniques*. Sensors and Actuators B: Chemical, 2012. **163**(1): p. 159-164.
7. Ramizy, A., Z. Hassan, and K. Omar, *Porous GaN on Si(100) and its application to hydrogen gas sensor*. Sensors and Actuators B: Chemical, 2011. **155**(2): p. 699-708.
8. Guo, X.Y., W. T.L., and B. P.W, *Enhanced ultraviolet photoconductivity in porous GaN prepared by metal-assisted electroless etching*. Solid State Communication, 2006. **140**: p. 159-162.
9. Luo, X., et al., *The ethanol-sensing properties of porous GaN nanofibers synthesized by electrospinning*. Sensors and Actuators B: Chemical, 2014. **202**(0): p. 1010-1018.
10. Williamson, T.L., et al., *Porous GaN as a Template to Produce Surface-Enhanced Raman Scattering-Active Surfaces*. The Journal of Physical Chemistry B, 2010. **114**(43): p. 20186-20191.
11. Youtsey, C., et al., *Smooth n-type GaN surfaces by photoenhanced wet etching*. Applied Physics Letters, 1998. **72**(5): p. 560-562.
12. Mynbaeva, M., et al., *Photoconductivity in Porous GaN Layers*. physica status solidi (b), 2001. **228**(2): p. 589-592.
13. Mahmood, A., et al., *Enhanced Properties Of Porous GaN Prepared By UV Assisted Electrochemical Etching* Advanced Materials Research, 2012. **364**: p. 90-94.
14. Mahmood, A., et al., *Characteristics of undoped porous GaN prepared by UV assisted electrochemical etching*. Optoelectron. Adv. Mater. Rapid Comm. , 2010. **4**: p. 1316-1320.
15. Vaipyei, A.P., et al., *High optical quality nanoporous GaN prepared by photoelectrochemical etching*. Electrochemical Solid State Lett., 2005. **8**: p. G-85G88.
16. Mynbaeva, M., et al., *Structural characterization and strain relaxation in porous GaN layers*. Applied Physics Letters, 2000. **76**(9): p. 1113-1115.

17. Mahmood, A., et al., *Effect of Porosity on the Characteristics of GaN Grown on Sapphire*. Conference Proceedings, 2011. **1341**(1): p. 45-47.
18. Mahmood, A., et al., *A Novel AC Technique for High Quality Porous GaN*. International Journal of Electrochemical Science, 2013. **8**.
19. Mahmood, A., et al., *The Role of Alternating Current on Photo-Assisted Electrochemical Porosification of GaN*. Journal of Nanoelectronics and Optoelectronics, 2014. **9**(2): p. 287-290.
20. Trichas, E., et al., *Selective photochemical etching of GaN films and laser lift-off for microcavity fabrication*. . Physica Status Solidi (a), 2008. **205**: p. 2509-2512.
21. Hartono, H., et al., *Annihilation of threading dislocations in strain relaxed nano-porous GaN template for high quality GaN growth* Phys. Stat. Sol. (c), 2007. **4**(7): p. 2572.
22. Yam, F.K., Z. Hassan, and S.S. Ng, *Porous GaN prepared by UV assisted electrochemical etching*. Thin Solid Films, 2007. **515**(7–8): p. 3469-3474.

Some Physical Properties of Turkey Berry (*Solanum Torvum*) Fruits

Mohd Haris Ridzuan Ooi Abdullah¹, Ch'ng Pei Eng², Mohd Firdaus Roslan³

¹Department of Applied Sciences, Universiti Teknologi MARA (UiTM) Cawangan Pulau Pinang,
13500 Permatang Pauh, Pulau Pinang, Malaysia

²Department of Computer and Mathematical Sciences, Universiti Teknologi MARA (UiTM) Cawangan Pulau Pinang,
13500 Permatang Pauh, Pulau Pinang, Malaysia

³Faculty of Chemical Engineering, Universiti Teknologi MARA (UiTM) Cawangan Pulau Pinang,
13500 Permatang Pauh, Pulau Pinang, Malaysia

(E-mail: harisridzuan@gmail.com)

ABSTRACT - Some physical properties of Turkey Berry (*Solanum Torvum*) fruits at moisture content of 81.86% (wet basis) are presented in this paper. They consist of the mean length, width, thickness, geometric mean diameter, sphericity, aspect ratio, unit mass, surface area and bulk density of the fruits. The mean length, width and thickness of the fruits were 11.59 mm, 11.65 mm and 11.42 mm, respectively. The average value for geometric mean diameter, sphericity, aspect ratio, mass, surface area and bulk density were 11.55 mm, 99.73%, 100.58%, 0.897 g, 420.39 mm² and 383.04 kg m⁻³, respectively. The coefficient of static friction on four types of structural surface was found to ranging from 0.162 (galvanized steel sheet) to 0.332 (rubber). The data are essential in the field of food engineering especially when dealing with design and development of machines, and equipment for processing and handling of turkey berry fruits.

Keywords: Physical properties, Turkey berry, *Solanum Torvum*.

1. INTRODUCTION

Solanum torvum is a small shrub commonly known as turkey berry in Africa, Asia, and South America. Turkey berry is an erect spiny shrub of about 4 meters tall, widely branched and stems armed with stout. The fruit becomes yellow when ripe. Categorized as one of the eggplants species, its edible fruits, commonly available in the market are used as a vegetable. Central and South America is the native habitat for turkey berry before it was cultivated and planted widely in the other countries. Most of the local people in West and Central Africa make the turkey berry as kitchen garden crop where they plant it in front or at the back of their houses [1]. In West Africa, turkey berry fruits becoming a famous daily vegetable, especially in Ghana [1]. The local inhabitants collect turkey berry fruits from home gardens and in the wild. In southern and eastern Asia, turkey berry was cultivated as a small-scale vegetable especially in Thailand. Turkey berry fruit is also a necessity in adding flavors to the Malays and Thai foods recipe and cuisines. Besides that, turkey berry fruits also serve as vegetables to the population's diet in the South Indian [2]. The local population in the South of China used its roots as folk medicine to treat gasteralgia, furuncle, trauma and fever. Many researchers had studied physical and mechanical

properties of various types of fruits and vegetables. These include orange [3], date [4], bergamot [5], velvet tamarind [6] and carrot [7]. However, the physical properties of turkey berry fruits were not reported. Currently, the harvesting and processing of turkey berry fruits was done manually and time consuming. In order to design machines and equipment for handling, processing and storing of the turkey berry fruits, the physical properties need to be studied and evaluated. The objectives of this study are to determine some physical properties of turkey berry fruits which could be useful in facilitating the design of machines to handle the process and storage of the fruits.

2. EXPERIMENTAL METHOD

Fresh turkey berry fruits were purchased from a wet market in Bukit Mertajam town located in Penang, Malaysia. The fruits were detached from the stalk. Foreign materials, immature and damaged fruits were removed from the sample. By using the ASAE standard method [8], the moisture content of the fruits was determined. The fruits were dried in an air ventilated oven at 80°C for 3 days. The wet basis was calculated as:

$$MC (\%) = \frac{mi-md}{mi} \quad (1)$$

Where MC (%) is the percentages of the moisture content, mi is the initial mass and md is the final mass of the fruits. The length (L), width (W) and thickness (T) of 100 seed were measures using a digital vernier calliper (Model CD-6BS-Mitutoyo Corporation, Japan) with resolution of 0.01 mm. The measurements for each dimension were repeated 100 times. Geometric mean diameter (D) was found using the following equation [9]:

$$D = (LWT)^{\frac{1}{3}} \quad (2)$$

Sphericity, S is defined as the ratio of the surface area of a sphere having the same volume as the fruit to the surface area of the fruit. The sphericity was determined using the following expression [9]:

$$S = \frac{(LWT)^{\frac{1}{3}}}{L} \quad (3)$$

In order to gather more information about the shape of the fruit, aspect ratio, R of the fruit was determined from the following relationship [10]:

$$R = \frac{W}{L} \times 100\% \quad (4)$$

The mass of 100 individual fruits was measured using an electronic balance (Model PS200/2000/C/2-RADWAG, Poland) with accuracy of 0.001 g. Surface area, A was calculated using the formula [11]:

$$A = \pi D^2 \quad (5)$$

The bulk density (ρ_b) was determined using the standard method [12] by filling and empty 100 mL beaker container with turkey berry fruits. The fruits were poured from a constant height until full at the top level and weighing. Bulk density was calculated as:

$$\rho_b = \frac{m_B}{V_B} \quad (6)$$

where, m_B = mass of fruits (g) and V_B = volume of container (m^3).

The coefficient of static friction (μ_s) were determined on four different type of surfaces, namely glass, plywood, rubber and galvanized steel sheet. The fruit was placed on the surface and was raised gradually until the fruit begin to slide. The angle of inclination at which the sample started sliding was measured using the protractor with accuracy of one degree. The coefficient of static friction was calculated using the following equation [4]:

$$\mu_s = \tan \theta \quad (7)$$

Where, θ = angle that the incline makes with the horizontal when sliding begins.

3. RESULTS AND DISCUSSION

Some physical properties of turkey berry fruits obtained in this study were shown in Table 1. The moisture content (wet basis) of the fruits was found to be in the range of 75.68 – 90.09 % with a mean moisture content of 81.86%. The storability of fruit depends on its moisture content. The higher the moisture content, the shorter the storage life of the fruit would be due to the rapid

growth of mould on the fruit. The mean value of length, width and thickness of the fruits were 11.59 (± 0.74), 11.65 (± 0.75), and 11.42 (± 0.62) mm, respectively. The dimensions of turkey berry fruits were found to be lower than bergamot [5] and orange [3]. The dimensions are important in determining the aperture size of machines, particularly in separation of materials [13]. These dimensions can be used in designing machine components and parameters as well as in estimating the number of fruits to be engaged at a time. The geometric mean diameter of turkey berry fruits ranges from 9.49 to 12.84 mm with a mean value of 11.55 (± 0.66) mm. The geometric mean diameter obtained can be used to determine the volume and sphericity of the fruit. The mean of sphericity and aspect ratio of the fruits were found to be 99.73 (± 1.89) % and 100.58 (± 3.32) %, respectively, while the mean mass of the fruits was 0.897 (± 0.146) g. The high sphericity and aspect ratio of the fruits indicate that the turkey berry fruit is likely to roll on their surfaces rather than slide. The sphericity was higher compared to *Juniperus drupacea* fruits [14], bergamot [5] and orange [3]. This parameter is of utmost importance in designing of hopper to handle the fruits. The average surface area of turkey berry fruits was found to be 420.39 (± 47.12) mm² and its mean bulk density was 383.04 (± 15.65) kg m⁻³. The information about bulk density of fruits is useful in determining the fruits storage capacity. The data obtained in this study shows that the bulk density of turkey berry fruits is higher than *Juniperus drupacea* fruits [14] and orange [3]. The smaller size of turkey berry fruits may have contributed to the higher value of bulk density. The coefficient of static friction of turkey berry fruits against four different types of structural surface was shown in Table 2. The mean coefficient of static friction for turkey berry fruits was generally higher than that of *Juniperus drupacea* fruits [14] than but lower than *Parkia speciosa* seeds [15]. The low value of coefficient of static friction may be attributed to the smoother surface of the fruit. It was found that the fruit had the highest coefficient of static friction on rubber and plywood, followed by glass and the least for galvanized steel sheet. This property is crucial in determining the steepness of the storage container, hopper or any other loading and unloading device.

Table 1. Some Physical Properties of Turkey Berry

Physical Properties	Unit of Measurement	No. of Observation	Mean Value	Standard Deviation
Length	mm	100	11.59	0.74
Width	mm	100	11.65	0.75
Thickness	mm	100	11.42	0.62
Geometric Mean Diameter	mm	100	11.55	0.66
Sphericity	%	100	99.73	1.89
Aspect Ratio	%	100	100.58	3.32
Mass	g	100	0.897	0.146
Surface Area	mm ²	100	420.39	47.12
Bulk Density	kg m ⁻³	10	383.04	15.65

Table 2. Coefficient of Static Friction on Four Types of Structural Surfaces

Coefficient of Static Friction Surface	No. of Observation	Mean Value	Standard Deviation
Plywood	30	0.201	0.033
Galvanized steel sheet	30	0.162	0.023
Rubber	30	0.332	0.057
Glass	30	0.189	0.039

4. CONCLUSION

The average moisture content (wet basis) of the turkey berry fruits determined in this study was 81.86 (± 5.65) %. The mean of length, width and thickness of the fruits was 11.59 (± 0.74), 11.65 (± 0.75) and 11.42 (± 0.62) mm respectively. The average value for geometric mean diameter, sphericity, aspect ratio, mass, surface area and bulk density was 11.55 (± 0.66) mm, 99.73 (± 1.89) %, 100.58 (± 3.32) %, 0.897 (± 0.146) g, 420.39 (± 47.12) mm² and 383.04 (± 15.65) kgm⁻³ respectively. The coefficient of static friction on four types of structural surface was found to be vary from 0.162 (± 0.023) for galvanized steel sheet to 0.332 (± 0.057) for rubber. The physical properties data obtained in this study can be useful in the design of machine and equipment for handling, processing and storing of the turkey berry fruits.

5. REFERENCES

1. Grubben, G. J. H. Plant Resources of Tropical Africa 2 G. J. H. Grubben & O. A. Denton (Eds.). Vegetables, 2004, p. 501-503.
2. Jaiswal, B.S. Solanum Torvum: A Review of Its Traditonal Uses, Phytochemistry and Pharmacology. International Journal of Pharma and Bio Sciences, 2012, p. 104-111. www.ijpbs.net
3. Sharifi, M., Rafiee, S., Keyhani, A., Jafari, A., Mobli, H., Rajabipour, A., & Akram, A. Some physical properties of orange (var. Tompson). Int. Agrophysics, 2007, p. 391-397.
4. Jahromi, M.K., Rafiee, S., Jafari, A., Bousejin, M. R. G., Mirasheh R., and Mohtasebi, S. S. Some physical properties of date fruit (cv. Dairi). Int. Agrophysics, 2008, p. 221-224.
5. Rafiee, S., Jahromi, M.K., Jafari, A., Sharifi, M., Mirasheh, R., & Mobli, H. Determining some physical properties of bergamot (Citrus medica). Int. Agrophysics, 2007, p. 293-297.
6. Asoiro, F. U., Ezeoha, S. L., Ugwu, C. B., & Ezenne, G. I. (2017). Physical properties of unshelled, shelled and kernel of velvet tamarind (Dialium guineense) fruit from Nigeria. Cogent Food & Agriculture, 3(1), 1287618.

7. Jahanbakhshi, A., Abbaspour-Gilandeh, Y., & Gundoshmian, T. M. (2018). Determination of physical and mechanical properties of carrot in order to reduce waste during harvesting and post-harvesting. *Food Science & Nutrition*.
8. ASAE Standard, 2003. *Moisture Measurement of Ungrounded Grain and Seed*. ASAE Press, St. Joseph, MI USA.
9. Mohsenin, N. N. *Physical Properties of Plant and Animal Materials*. Gordon and Breach Science Publishers, New York, USA, 1970.
10. Maduako, J. K., & Faborode, M. O. Some physical properties of cocoa pods in relation to primary processing. *Ife J. Technol*, 1990, p. 1-7.
11. McCabe, W. L., Smith J. C., and Harriot, P. *Unit Operations of Chemical Engineering*. McGraw-Hill Press. New York, USA, 1986.
12. Fraser, B. M., Verma, S. S., and Muir, W. E. Some physical properties of fanabeans. *Journal of Agricultural Engineering Research*. 1978, 22: 53–57.
13. Mohsenin, N.M. *Physical Properties of Plant and Animal Materials* New York, USA: Gordon and Breach Science Publishers, 1986.
14. Akinci, I., Ozdemir, F., Topuz, A., Kabas, O., and Canakci, M. Some physical and nutritional properties of *Juniperus drupacea* fruits. *J. Food Eng*, 2004, p. 325-331.
15. Abdullah M.H.R.O., Ch'ng P.E. & Lim T.H. Some physical properties of *Parkia speciosa* seeds. *IACSIT Press*, 2011. p. 43-47.

Cogitation of Structural and Morphology Properties of Porous Silicon.

Mohd Bukhari Md Yunus, Sharifah Nooraishah Syed Mohd Zainol, Mohd Zaki Mohd Yusoff, Muhammad Firdaus Othman

Department of Applied Sciences, Universiti Teknologi MARA Cawangan Pulau Pinang,

Jalan Permatang Pauh, 13500 Permatang Pauh, Pulau Pinang Malaysia

*Corresponding e-mail: bukhari.myunus@ppinang.uitm.edu.my

ABSTRACT - This paper present a simple and economical, yet reliable technique to fabricate porous silicon (PS) which is electrochemical etching. Studies on PS have indicated the structural properties and morphological of its surface depends on etching time. PS was anodized in presence of light source for 7, 10 and 13 minutes at 30 – 35 mA/cm² current densities range in 1:4 hydrofluoric acid (49%) and ethanol (99%) act as an electrolyte. Detailed information about evolution of PS morphology with variation preparation condition was obtained by field emission scanning electron microscopy (FESEM) that occupied with energy dispersive x-ray (EDX) and atomic force microscopy (AFM). The results shows that n-type porous silicon surface featured three-branched shape pores as the branches are connected each other in discrete location whereas p-type porous silicon featured an irregular shape was confirmed using FESEM. The control of these properties was shown to depend on etching time. Based on EDX analysis, it represents the element presence on PS surface layer that affect the degree of porosity. In AFM analysis, the root mean square (rms) roughness of PS layer is found to be decreased from 0.187 μm to 0.0352 μm for n-type silicon and for p-type silicon 0.0239 μm to 0.0159 μm due to the increasing of etching time. The etching process, structural properties and morphology of PS formed is briefly described and can be better defined due to the improved passivating nature of wafer surface.

Keywords : porous silicon, electrochemical etching, morphology, etching time

1. INTRODUCTION

Porous silicon has attracted increasing interest for various applications including photonics, electronic and biosensing since it was first discovered by Arthur Uhlirs in 1956. PS is normally formed by electrochemical etching of silicon wafer in hydrofluoric acid-based solution. Through the electrochemical etching process, PS can display different morphologies depend on the formation parameter (Rusli, 2013). The physical properties of PS are fundamentally determined by the shape, diameter of pores, porosity and the thickness formed of the porous silicon layer (Kumar&Huber, 2007). For instances, by controlling the size and orientation of the pores, it can be manufactured to have specifically designed optical, electrical, mechanical, thermal and chemical characteristics. PS which is a nano structured material usually defines as one tenth of micrometer in at least one dimension. In addition, the important aspects those being considered in this material are the wide increase surface area to volume ratio of material in nano size material. This aspect make the nano scale material experiencing quantum confinement effects

that happen when the silicon is being etched, some of their parts are being removed. The well-studied of PS morphology can range from ≤ 2 nm for microporous, 2 to 50 nm for mesoporous to the macroporous, > 50 nm of pore width with a sponge-like structure formed in silicon consisting of a finely connected network of submicron silicon thread (Perez, 2007).

The major reasons that have contributed to the widespread attention given to the porous silicon are its production is simple and inexpensive compare to the current technique used to produce low dimensional structures. Its compatibility with current silicon microelectronic processing makes integrated silicon based optoelectronic devices a possibility. It is very large surface area to volume ratio makes the porous silicon matrix an excellent host for chemical and biological species. Many favorable characteristics and the vast interest in porous silicon have given rise to a variety of new application such as photodetector.

The variation in the obtained results by previous researchers confirms the difficulties exist when it comes to effectively controlling the pore formation. According to the studies done by Matoussi et al. (2008), surface morphology and the GaN grown on the surface of silicon were described for its optical properties. The formation of highly doped n-type porous silicon utilizing short etching time and high current densities is described by Yaakob et al. in 2013. However, in the formation of porous silicon, stochastic model silicon electrochemistry was used that in guiding experimental design for specific pore formation (Foll et al., 2002). As the pore formation, the thickness and porosity were measured using gravimetric method (Hadi, 2013 ; Behzad, 2012). Moreover, regarding to the various mechanism of the pore formation and several different model on the chemical dissolution have been independently suggested (Parkhutik, 1999 ; Rusli, 2013). The morphological change in shape, size of pores and porous layer thickness due to the change of etching time was observed using FESEM.

2. EXPERIMENTAL PROCEDURE

The n-type (111) and p-type (111) silicon wafer of 256-306 μm thickness and has specific resistance of 1-10 ohm.cm resistivity was used to fabricate porous structures. Prior to etching process, all samples that were cut into 1.2 cm X 1.2 cm were cleaned using standard RCA cleaning. The electrochemical process were performed in Teflon by using two electrode configurations with platinum rod as cathode as it is inert and does not react with aqueous electrolyte and aluminium plate as anode as shown in figure 1. The polished surface of the silicon was exposed to the electrolyte whilst the back-side of the silicon was attached to the aluminium plate. A mixture of the 49% hydrofluoric acid and 99% ethanol with a volume ratio

of 1:4 was used as an electrolyte. PS samples were prepared for various etching times of 7, 10 and 13 minutes at current densities between 30-35 mA/cm². This process was conducted under source of light in order to generate more holes (Rusli, 2013). After the etching process, PS samples were rinse with de-ionized water and dried in the ambient air. Then, it was stored in the sealed container to prevent contamination. The resulting PS layers were characterized by field emission scanning electron microscopy (FESEM) that comes with energy dispersive x-ray (EDX) component and atomic force microscopy (AFM) in term of pore morphology and root mean square roughness surface of the sample.

3. RESULTS AND DISCUSSION

The dependence of the pore dimension and pore geometry of PS surface in 7, 10 and 13 minutes etching time has been determined from the FESEM images with 25 000 magnification. Figure 2 and 3 shows n-type and p-type porous silicon FESEM surface images PS formed at etching time 7 minutes and 13 minutes.

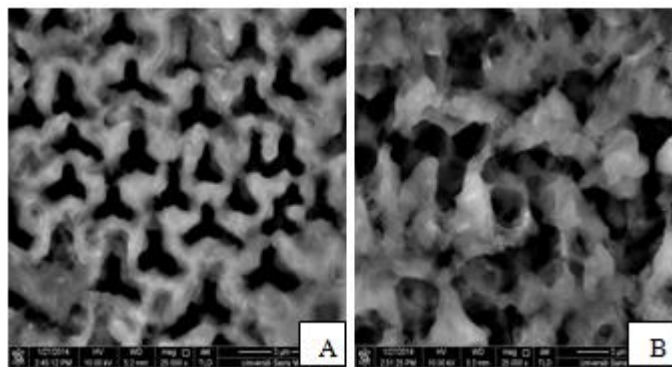


FIGURE 2: FESEM Surface Images Of N-Type Silicon A) 7 Minutes B)13 Minutes

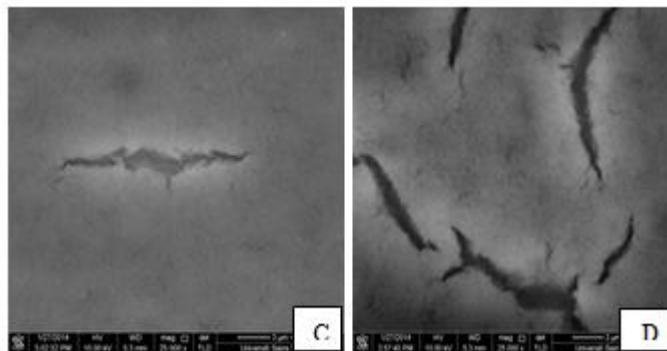


FIGURE 3: FESEM Surface Images Of P-Type Silicon A) 7 Minutes B)13 Minutes

The FESEM surface image of PS formed that has being taken by using FESEM, give an ultra-high resolution image. The period of etching time would shows the level of porosity and allow us to identify morphology and structural properties of the sample. As shown from the image (a), three-branch-shaped pores with various sizes can be clearly observed at discrete locations. The branches are almost on equal size and spread through the area. This shows that the sample has a uniformly porous surface. This is in agreement with the work of Rusli et al., who prepared low doped n-type silicon with an etching time range time from 20 to 60 min at constant current density 25 mA/cm^2 . The difference in porosity can be seen clearly from the image when the etching time is longer. The surface of image (b), PS samples also possess high degree of porosity with randomly distributed three-branch-shaped pores. An increasing of etching time from 7 minutes to 13 minutes leads to the formation of highly connected three-branched-shaped pores.

Based on the observation between two image of 7 minutes and 13 minutes of 111 n-type porous silicon, the longer the time etching process, the pore diameter is also increases. The increment in pore diameter of the former case was the result of active dissolution of Si at the pore wall which enlarged the pore size, and consequently reduced the inter-pore distance. This is in agreement with the results reported by other studies (Yaakob et al., 2012). Inter-pore distance becomes narrower with an increasing etching time. This may due to the fast dissolution on the Si surface via a direct attack of HF followed by oxidation. Once the pores were formed, the remaining surface Si became inert from further direct dissolution, leading to the observed constant pore density and pore diameter. Then, if a rapid dissolution continuing with longer etching times caused the pore wall to break.

The surface of image (c) shows that pore is not clearly seen because it is about to develop. The small crack indicates this type of silicon is difficult to fabricate due to short etching time. Results also demonstrate that there is no apparent effect of the etching time on the pore shape when there is only a region that the silicon is being etched. In the FESEM surface image (d) shows that the etching reaction occurred on the Si surface homogeneously. The pores are irregular in shape, and are randomly distributed on the PS surface. Inter-pore connection is low between one pore to another. Based on the results of (c) and (d) images, it shows that the surface of silicon is poor contact with the electrolyte causes etching did not occur on certain region. However, based on previous research of Hecini et al. in 2013, it portrays that cross sectional of PS of p-type that results with a long void running perpendicular to the surface, with occasional branches and numerous small buds on the side of the main pores with the same electrolyte concentration at 15 mA/cm^2 for 5 minutes etching time. The degree of branching and inter-pore connection depends strongly on doping concentration. The most highly connected PS is found in

the low-doped p-type silicon whereas well separated PS generally found on moderately doped n-type silicon. Variations in the morphology of the PS regions were mainly due to the effect of the Si dissolution process, which occurred at the silicon electrolyte interface. Based on EDX analysis, it shows that carbon and oxide element have deposited on the n-type PS whereas on p-type PS has only oxide layer deposited on the surface. By this existence, it affects the formation PS as the deposited element form a thick layer on the surface.

Figure 4 below shows the representative atomic force microscopy (AFM) images corresponding to PS prepared at etching times of 10 minutes and 13 minutes.

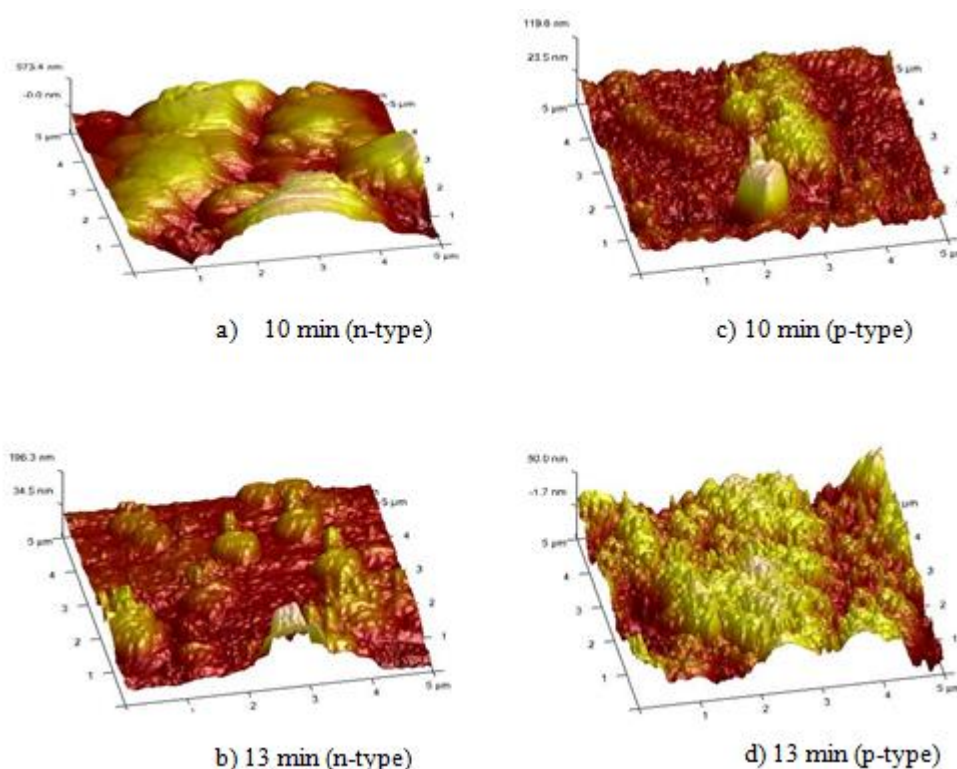


FIGURE 4: AFM images of PS surface formed as a function of etching time.

Electrochemical etching during the production of PS generated several small bumps on the surface. The formation of such bumps is possibly due to the surface relief of the Si nanostructures after the etching process. The number of bumps on the surface of the PS gradually increased with the etching time. A plot of the roughness value (rms) of the PS surface as a function of the etching time shows in figure 4. As the etching time was prolonged, the surface roughness decreased from $0.187\mu\text{m}$ to $0.0352\mu\text{m}$ of n-type porous silicon and $0.0239\mu\text{m}$ to $0.0159\mu\text{m}$ of p-type porous silicon corresponding to applied current density between $30\text{-}35\text{ mA/cm}^2$. Value of roughness depends on the experimental parameter such as etching rate, HF

concentration and many more. The smoothening of PS surface due to prolong etching time that results the bump is not uniform in height. However, from previous studies of Rusli et al. results the increasing number of these uniform height of bump that by cause the amount of their non-uniform counterparts to decrease. The lower the surface roughness indicates that the higher porosity of PS formed and higher density of pores. According to the previous studies of Nayef and Muayad et al. in 2013, it has similarities with the current result of p-type silicon in three dimensions image but in this studies, state that in two dimension images, a sponge-like structure is produced The surface of the sample was consisted of numerous tiny pores formed over the soft wall.

4. CONCLUSION

In conclusion, PS samples were prepared by electrochemical etching method under current densities between 30 – 35 mA/cm² and three different etching times. The studies of dependence of porosity and thickness of samples on the current density and etching time have been done. The porosity increase rapidly as the overall thickness also increases due to the long period of etching time. For the effect of etching time, 7, 10 and 13 minutes is sufficient time for silicon to fabricate and increase the porosity with the presence source of light. The longer the etching time, the higher the porosity formed on PS surface. Moreover, with the range of current densities between 30 – 35 mA/cm² results in the widening of the pore size depends on the period of etching time. The morphology of PS formed changed from the uniform three-branched shape pore at 7 minutes to randomly three-branched shape pore at 13 minutes with the increases of the inter-pore connection. Upon increasing the etching time from 10 minutes and 13 minutes, the PS surface roughness decrease from 0.187 μm to 0.0352 μm. A basic investigation into the electrochemical etching of both n-type and p-type silicon is performed as the consistent direct electrochemical dissolution propagated pores into the bulk Si with occasional branching as the etching time was increased. Since nanostructure PS increases in the surface area to volume ratio as it experiences quantum confinement effects. This is because of the reduction in dimension of PS when the silicon is being etched. Although this work was only focused on the morphological and structural properties of PS formed at prolonged etching time, it is hoped that explanation will some insight on the formation of PS and its corresponding mechanisms.

ACKNOWLEDGEMENT

Special thanks to supervisor, En. Mohd Bukhari Md Yunus, co-supervisor, Pn. Alhan Farhanah Abdul Rahim, department of applied sciences and faculty of chemical engineering.

5. REFERENCE

- [1] Behzad,K., Yunus,W.M.M., Talib, Z.A., Zakaria,A.& Bahrami, A. (2012). Effect of preparation parameters on physical, thermal and optical properties of n-type porous silicon. *Journal of Electrochemical Science*. 7, 8266-8275.
- [2] Foll,H., Christopherson, M., Carstensen,J. & Hasse,G. (2002). Formation and application porous silicon. 39, 93-141.
- [3] Hadi,H.A., Ismail,R.A. & Habubi,N.F. (2013). Fabrication and characterization of porous silicon layer prepared by photo-electrochemical etching in CH₃OH:HF solution. *International Letters of Chemistry, Physics and Astronomy*. 3, 29-36.
- [4] Kumar,P. & Huber,P. (2007). Effect of etching parameter on pore size and porosity of electrochemically formed nanoporous silicon. *Journal of Nanomaterial*.2007,1-4.
- [5] Matoussi,A., Nasr,F.B., Salh,R. et al. (2008). Morphological, structural and optical properties of GaN grown on porous silicon/Si(100) substrate. *Material Letters*. 62,515-519.
- [6] Parkhutik,V. (1999). Porous silicon-mechanisms of growth and application. 43,1121-1141.
- [7] Perez,E.X. (2007). Design, fabrication and characterization of porous silicon multilayer of optical devices (pp. 5-26). Tarragona,Spain.
- [8] Rusli,N.I., Abidin,M.S.Z., Astuti,B., Ali,N.K. & Hashim, A.M. (2013). Formation of porous silicon: Mechanism of macropores formation of n-type Si. 42(5), 643-648.
- [9] Yaakob,S., Bakar,M.A., Ismai,J., Bakar,N.H.H.A. & Ibrahim,K. (2012). The formation and morphology of highly doped n-type porous silicon: effect of short etching time at high current density and evidence of simultaneous chemical and chemical dissolution. *Journal of Physical Science*. 23(2), 17-31.

LITHIUM ION CAPACITOR: ELECTROCHEMICAL PROPERTIES OF PRE-DOPING ELECTRODE BY USING TWO DIFFERENT COATING TECHNIQUES.

Nor Faranaz Shamin Nor Azmi^{1*}, Surani Buniran², Mohd Firdaus Roslee², Norha Abdul Hadi¹, Madhiyah Yahya¹, Siti Hajar Salleh¹, Masbudi Baharuddin³

¹ Department of Applied Sciences, UiTM Pulau Pinang, 13500 Permatang Pauh, Penang, MALAYSIA,

² Advance Material Research Centre, Sirim Berhad, Kulim Hi-Tech, 09000 Kulim, Kedah, MALAYSIA.

³ Faculty of Science and Technology, USIM, 71800 Nilai, Negeri Sembilan, MALAYSIA.

(E-mail: faranaz@ppinang.uitm.edu.my)

ABSTRACT - Pre-doping is a method to add Lithium containing compound into the positive electrode of lithium ion capacitor (LIC). The objective of this research is to evaluate which composition of LiFePO_4 will enhanced the electrochemical performance of LIC. To investigate electrochemical performance of two different coating method, the positive and negative electrode were prepared by coating the slurry on the steel mesh. Meso-carbon microbeads (MCMB) were selected as the negative electrode material, and it was prepared by impregnate the steel mesh with slurry of MCMB, carbon black and PVDF (85:10:5) which dissolved in NMP. On the other hand, activated carbon (AC) was used as the positive electrode. The LiFePO_4 was used as lithium containing compound and was added into the AC positive electrode with different proportions (0 wt. %, 5 wt. %, 10 wt. %, 15 wt. %, 20 wt. %, and 25 wt. %). Both electrode were assembled in glove box by using polypropylene (PP) microporous sheet as separator, and 1M LiPF_6 was dissolved in ethyl carbonate (EC) and dimethyl carbonate (DMC) as electrolytes. The process was continued by coating the slurry by using k-paint applicator. Then the positive electrode was prepared by coating slurries containing active material and binder, PVDF dissolved in NMP on aluminium foil. While, the negative electrode was prepared similar way on copper foil with slurry of active material, conducting agent (carbon black) and PVDF. Both electrodes were dried at 900 °C for 24h. The results show that, higher performance of LIC is obtained when 20% of LiFePO_4 was added into the positive electrode which is 9 time higher energy density compared to the sample without LiFePO_4 and the energy density obtained by k-paint applicator is 74.6 Wh/kg, which is 7 times higher compared to the slurry paste in mesh.

Keywords: lithium ion capacitor; LiFePO_4 ; pre-doping method; lithium intercalation-de-intercalation; k-paint applicator.

1. INTRODUCTION

LIC is one of the hybrid type capacitors, which is a combination of lithium ion battery and Electrical Double Layer Capacitor, EDLC supercapacitor. It is one of the new inventions of EDLC supercapacitor. In general, EDLCs with symmetrical high surface area of activated carbon (AC) are consider as a promising energy storage device because they are capable to deliver high power in short periods of time. However, limitation of these EDLCs are their low energy storage or delivery capability relative to lithium-ion battery [1]. The approaching method to overcome this limitation of EDLCs are by replacing the negative AC electrode with a battery electrode known as the hybrid electrochemical capacitors. This new device obtains a larger energy density, higher power density and more stable performance. G.G Amatucci developed the first LIC by using a lithium ion intercalation based on $\text{Li}_4\text{Ti}_5\text{O}_{12}$ for negative electrode and activated carbon as the positive electrode [2]. The next generation of LIC using other carbonaceous material negative electrode such as graphite, activated carbon or meso-carbon microbeads (MCMB). The MCMB and graphite commonly used for the negative electrode of LIC because the capability of Lithium intercalation is higher at the surface of the negative electrode compared to AC [3].

As a hybrid supercapacitor, its function according to the principle operating of EDLC capacitor in the positive electrodes and the principle operations of lithium ion battery at their negative electrode [4]. When LIC is charged, lithium ions intercalated at the negative electrode and the anions are physically adsorbed at the positive electrode. When the lithium-ion capacitor is discharged, the lithium ions de-intercalating from the negative electrode and intercalate at the precise location on the positive electrode from which the anion has been desorb. The LIC shows different operating mechanism which the positive electrodes adopt the same physical adsorption mechanism as for the EDLC and the negative electrode is accompanied by the chemical reaction involving lithium ion pre-dope/discharged just as the material of the lithium ion battery negative electrode [5]. However, using carbonaceous material in negative electrode resulted in inevitable irreversible capacity loss (ICL) which prevents fully discharging of positive electrode [6], and leads to poor electrochemical performance and lower efficiency. To solve this problem, negative electrode doped by lithium ion commonly used. This negative electrode preliminary treatment is called the pre-doping [7]. In the conventional LIC, metallic lithium is incorporated to the cell package. During the charging process, lithium ions intercalated into the negative electrode. During the doping process, metallic lithium is oxidized to release lithium ion at the negative electrode surface. Even though this Li-pre doping process can lower the negative electrode potential and improve the LIC working voltage, but it would be difficult to load the amount of desired lithium precisely because of the loaded metallic lithium cannot be fully inserted into the negative electrode material. The remaining metallic lithium in the LIC leads to the shrinking of energy density. This is because of the increase in weight leads to the increase in potential safety problems and could worsen the production technology [8].

In this work, the similar pre-doping method introduced by Feng Wu [8] was conducted. This method suggests that, instead of using lithium metal in conventional LIC, lithium containing compound/lithium metal oxide were simply added and inserted into the positive electrode. When the capacitor is charged, lithium ion will released from lithium containing compound/lithium metal oxide into the electrolyte and lithium ion in the electrolyte were intercalated into the negative electrode. This mechanism has the same effect as the pre-doping in the conventional LIC. Besides, in this method, the negative electrode ICL was reduced or compensated by lithium ion from lithium containing compound/lithium metal oxide which may improve the coulombic efficiency and leads to the enhanced electrochemical performance in LIC. In the other hand, by using this new pre-doping method, the amount of excessive lithium ion can be controlled by varying the amount of lithium containing compound/lithium metal oxide added in the positive electrode [8].

In this study, LiFePO_4 was chosen as lithium containing compound/lithium metal oxide because of its relatively low cost, high specific capacity (170mAh/g), good thermal stability, excellent cycling performance and nature safe [9]. In a complete cell, charging rates, voltage ranges and current densities are the important parameters to determine the electrochemical properties such as capacitance (F), specific capacitance (F/g), energy density (Whr/kg) and power density (W/kg). The equivalent capacitance can be obtained by using the equation (1) below,

$$\text{Capacitance, } C_{cell} = \frac{I}{\left(s, \left(\frac{dv}{dt}\right)\right) (\text{unit } F)} \quad (1)$$

where, I is the voltammetric average current $I = (I_a + I_c)/2$ and s is the scan rate [10].

Next, the specific capacitance of the 2 electrodes cell was calculated as follows:

$$C_s = \frac{2C_{cell}}{m} \left(\text{unit } \frac{F}{g} \right) \quad (2)$$

$$C_s = \frac{4C_{cell}}{M} \left(\text{unit } \frac{F}{g} \right) \quad (3)$$

Where, C_{cell} is the total capacitance of the cell (F), m is the mass of the activated material in one electrode (g), M is the total mass of the active material in both electrodes and C_s is the specific capacitance of the activated carbon [11]. The specific energy density of the supercapacitor can be calculated according to equation (4) as the quantity per unit mass or per unit volume.

$$E = \frac{1}{2} C_s (V_1 - V_2)^2 \left(\text{unit } \frac{Wh}{kg} \right) \quad (4)$$

where, V_1 and V_2 is the maximum and minimum working voltage [12].

2. EXPERIMENTAL METHOD

2.1 Preparation of the positive electrode with different percentage of LiFePO

First, the lithium containing compound (LiFePO_4) were added into the activated carbon positive electrode. Then, the positive electrodes were prepared by coating a stainless steel mesh with the slurry of AC+ LiFePO_4 , carbon black and PVDF (85:10:5) which dissolved in N-methyl-2-pyrrolidinone (NMP). The LiFePO_4 with different proportions (0 wt%, 5 wt%, 10 wt%, 15 wt%, 20 wt% and 25 wt%) were added into the activated carbon (AC) and labelled as S0, S5, S10, S15, S20 and S25 to mark the samples. Then, the samples were dried for 12 hours at 700 °C using vacuum oven. The negative electrodes were prepared by impregnate the steel mesh with slurry of MCMB, carbon black and PVDF (85:10:5) which dissolved in NMP. The negative electrode and positive electrode of LICs were assembled in a glove box. Polypropylene microporous sheet was used as separator and 1M LiPF₆ was dissolved in ethyl carbonate (EC) and dimethyl carbonate (DMC) as electrolyte. The detail of mass percentage for each samples are shown as in the Table 1 below.

Table 1: Percentage of material for positive electrode (AC).

Sample	S0	S5	S10	S15	S20	S25
LiFePO₄	0%	5%	10%	15%	20%	25%
Active Material	85%	80%	75%	70%	65%	60%
PTFE	15%	15%	15%	15%	15%	15%

The positive and negative electrodes were assembled in Teflon cell by using the glove box with 1M LiPF₆ (ethylene carbonate-dimethyl carbonate EC-DMC) as electrolyte and PP as separator. Using LiPF₆ as electrolyte has offered two advantages. Firstly, due to present of EC, it also displays a better solid electrolyte interphase (SEI), forming ability on carbon and secondly, it possesses a higher ionic conductivity, which is beneficial for high current cycling. Next, the experiment was proceeds by using various scan rate, current density and potential cut-off in order to get the best parameter to obtain the optimum performance of this LIC.

2.1.1 Mesh coating technique

At this stage, the positive and negative electrodes were be prepared by coating the slurry on the steel mesh. MCMB were selected as the negative electrode material while, AC was selected as positive electrode. This selection was made to study the total capacitance for LIC either by using mesh technique or applicator technique.

2.1.2 Applicator coating technique

The work was continued with the process of coating the slurry on the foil by using k-paint applicator technique (Dr. Blade). The positive electrodes were prepared by coating slurries containing active material and binder, PVDF dissolved in NMP on aluminium foil. The negative electrodes were prepared in the same way on csopper foil with slurry of active material, conducting agent (carbon black) and PVDF. Both electrodes were dried for 24h at 900 °C. Next, the electrodes were assembled in a glove box to avoid humidity and PP was used as separator. The detail of material is shown as in the Table 2. This sample then undergo cyclic voltammetry (CV) and charge-discharge (CD) processes in order to study the performance of its electrochemical properties. These samples are expected to obtain more higher energy density, higher specific capacitance but at lower resistance.

Table 2: The details of the sample

Sample I		Sample II	
Negative Electrode	Positive Electrode	Negative Electrode	Positive Electrode
MCMB(85%)	AC+ LiFePO ₄ (20%)	MCMB(85%)	MCMB + LiFePO ₄ (20%)

3. RESULTS AND DISCUSSION

The suitable conditions and analytical characteristics were shown in Table 1. Figure 1(a) - 1(f) shows the CD curves obtained for LIC using AC for positive electrode and MCMB as the negative electrode in which different proportions of LiFePO_4 were used and each cells were labeled as S0, S5, S10, S15, S20 and S25 with potential range of 2-3.5V at current density 50 mA/g (per mass of positive electrode). When the cell is charging, lithium ion intercalate into MCMB negative electrode, and simultaneously, double layer were formed at the surface of AC positive electrode due to adsorption of PF-6.

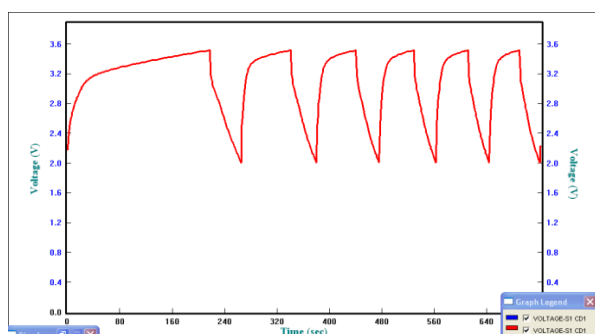


Figure 1(a): Charge-Discharge curve for S0 with current density 50 mA/g

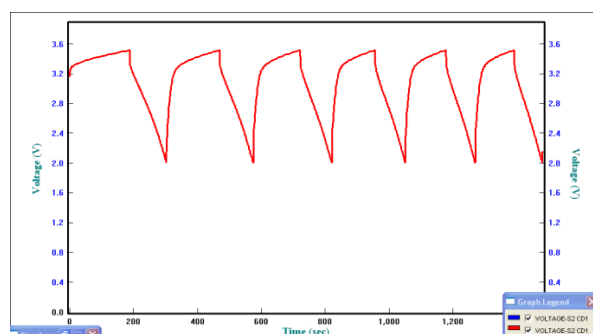


Figure 1(b): Charge-Discharge curve for S5 with current density 50 mA/g

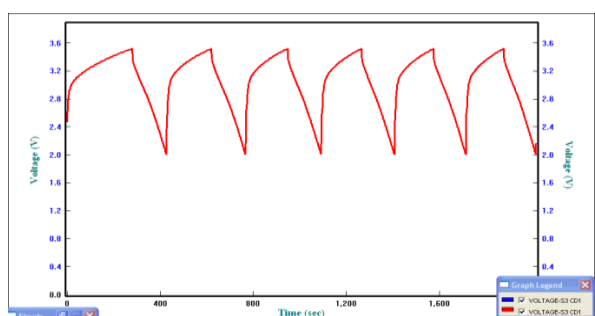


Figure 1(c): Charge-Discharge curve for S10 with current density 50 mA/g

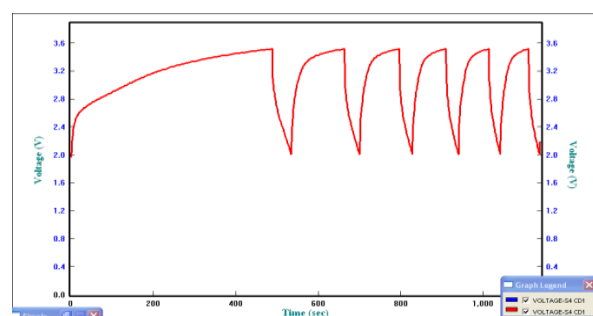


Figure 1(d): Charge-Discharge curve for S15 with current density 50 mA/g

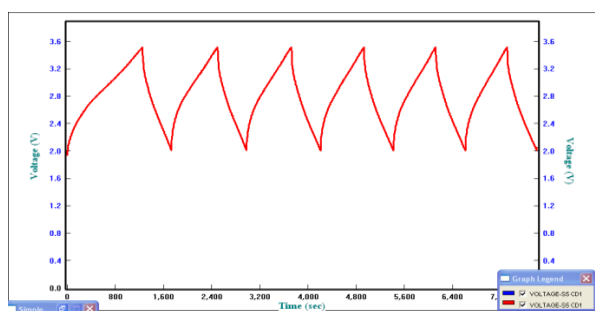


Figure 1(e): Charge-Discharge curve for S20 with current density 50 mA/g

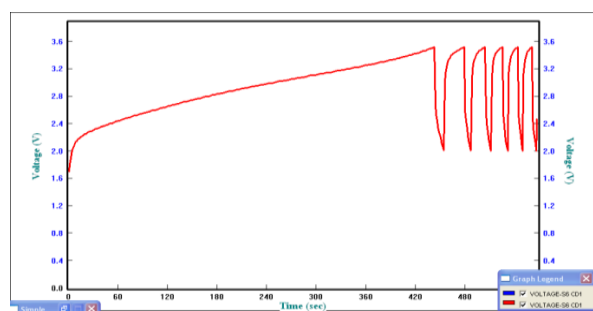


Figure 1(f): Charge-Discharge curve for S25 with current density 50 mA/g

From the Figure 1(a), we can observe that the discharge capacity of LIC is much lower than the charge capacity, indicates the extremely low coulombic efficiency. The absence of pre-doping made MCMB negative electrode possessed a high irreversible capacity and caused this low coulombic efficiency. Next figure reveals the trend that the charge-discharge curve become more symmetric with the addition on the quantity of LiFePO_4 into the positive electrode, and the capacitor electrochemical performance shows some improvement. But, for S15 and S25 reveals lower coulombic efficiency due to some irreversible capacity. From the entire charge-discharge figure, we can observe that the figure 1(e) shows the most symmetric and the highest electrochemical capacitor performance.

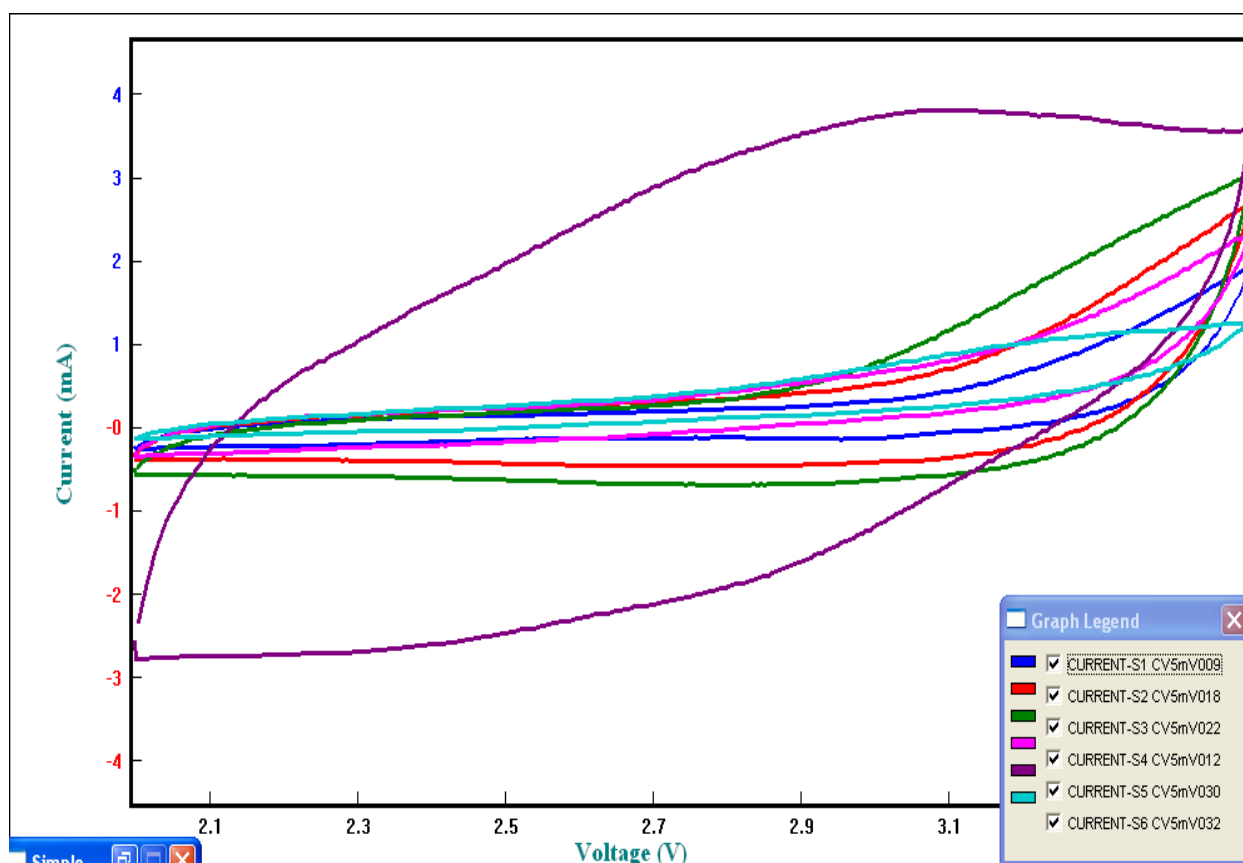


Figure 2: Cyclic Voltammetry curve for S0, S5, S10, S15, S20, S25. The scan rate for each sample is 5 mV/s with cut of potential 2-3.5 V.

The above Figure 2 shows the cyclic voltammetric pattern, which is S20 reveals the widest area under the curve and it is clearly shown that capacitor using AC with 20% LiFePO_4 has the best capacitance performance.

Table 3: Result analysis of different percentage lithium ion cell.

Sample	S0 (0%)	S5 (5%)	S10 (10%)	S15 (15%)	S20 (20%)	S25 (25%)
Current Density (50 mA/g)	1.210E-03	1.286E-03	1.348E-03	1.455E-03	1.465E-03	1.485E-03
Discharge Time (s)	52.2600	117.4272	159.4158	28.0338	478.6080	28.6698
Potential Cut Off (V)	1.4988	1.5002	1.5006	1.5011	1.5002	1.4951
Capacitance (F)	0.0422	0.1007	0.1432	0.0272	0.4674	0.0285
Specific Capacitance (F/g)	3.4868	7.8259	10.6235	1.9272	31.9029	1.9176
Energy Density (Wh/kg)	1.0896	2.4456	3.3198	0.6022	9.9697	0.5992

From Table 3, it lists the calculated capacitance, specific capacitance and energy density for samples S0 to S25. Since the negative electrode of MCMB is excessive, calculation of specific capacitance value is based on the mass of AC to evaluate the LIC performance. This result prove that sample S20 obtain the highest capacitance, specific capacitance and energy density compared to the other cells. The S20 obtain specific capacitance 10 times higher than S0 which is 31.9 F/g and enhance in energy density which is 89% compared to S0. This result is consistence with the results from Figure 1 and Figure 2. The results clearly show that the LIC performance was improved when certain amount of LiFePO₄ added into the positive electrode of AC.

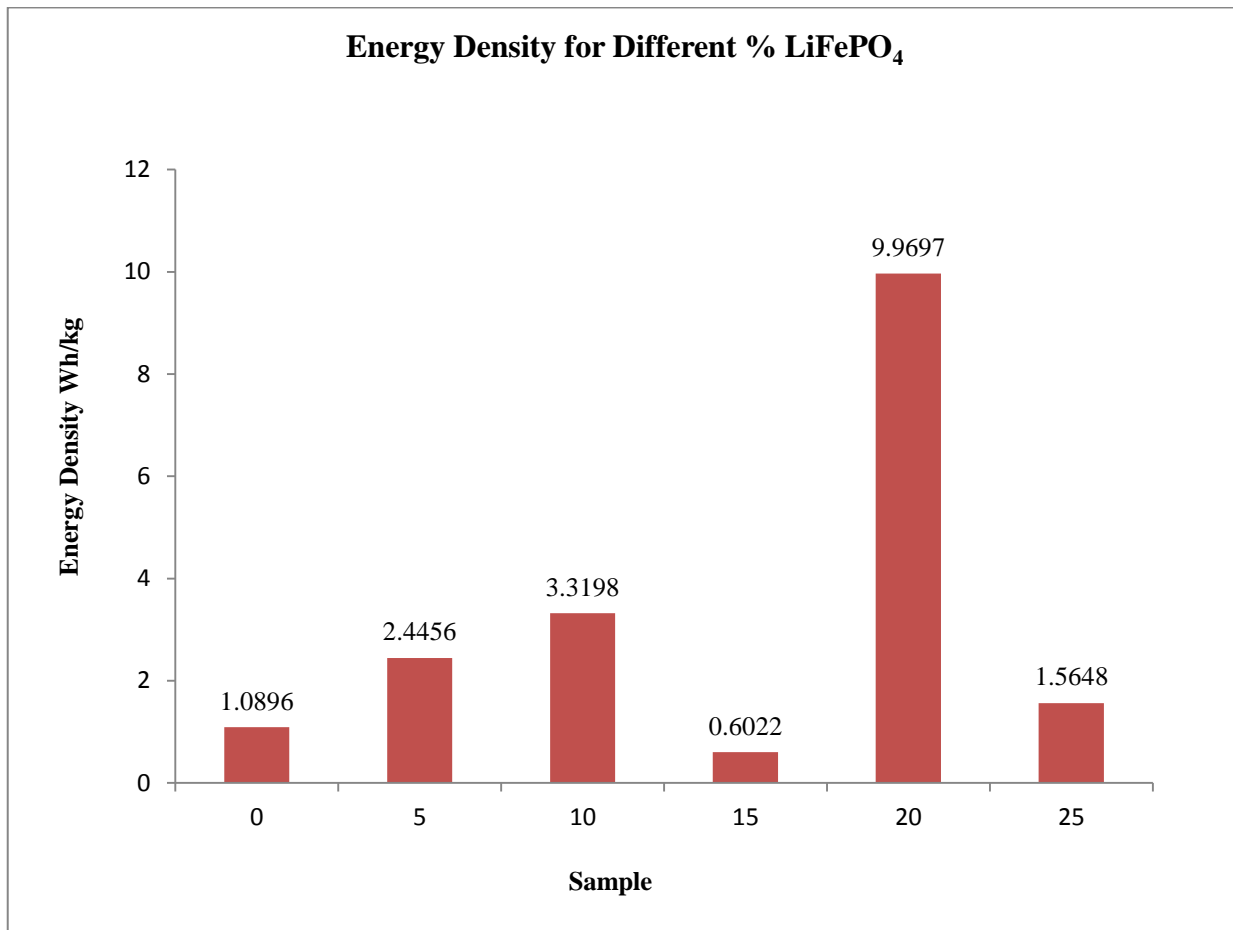


Figure 3: Energy density versus various percentage of sample.

Figure 3 shows the energy density for different samples with different percentage. It clearly show that the highest energy density is obtain when 20% of LiFePO_4 is added to the LIC positive electrode. As a result, to compensate its irreversible capacity of LiFePO_4 , 20% is the best amount. From this figure, we can say that this pre-doping technique is necessary to fulfil the conventional LIC system criteria, and the level of lithium doping can be controlled by adding the amount of LiFePO_4 at the positive electrode.

Dr.Blade technique gives almost the same result with mesh, but the advantage of this technique was the thickness of the electrode was very small which is at 100 μm . So, since the weight of electrode was really small, it contributes to high amount of capacitance and high energy density.

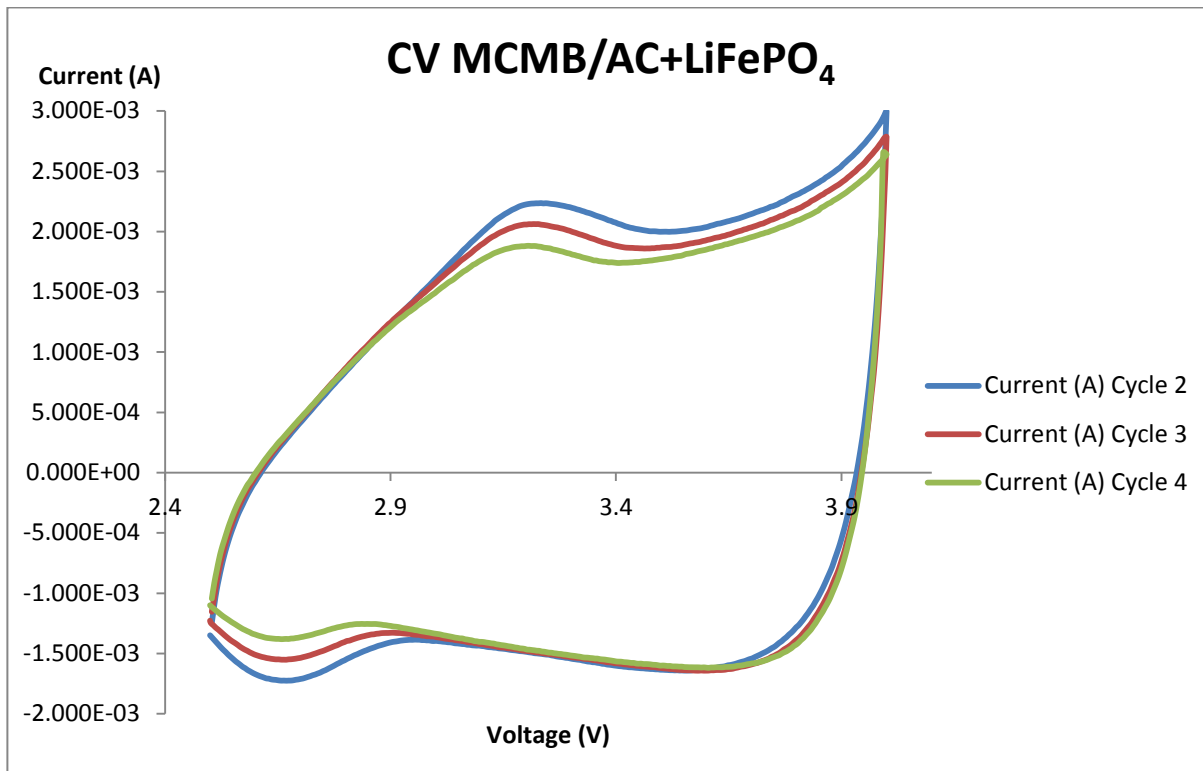


Figure 4: CV Curve for LIC with MCMB as -ve electrode and AC + LiFePO₄ as +ve electrode.

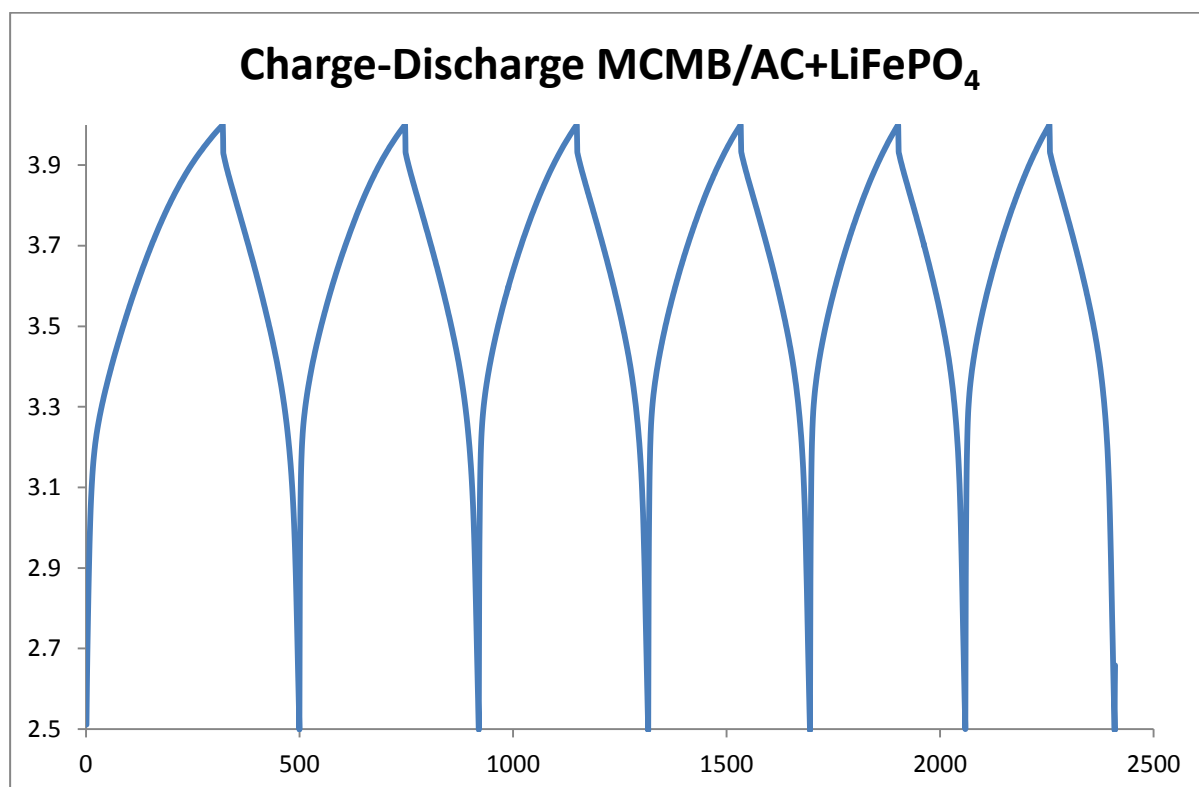


Figure 5: Charge-Discharge for LIC with MCMB as negative electrode and AC + LiFePO₄ as positive electrode.

From Figure 5, we can observe the two peaks in the charging and discharging process. During charging, there were small peak occur around from 3.1 V. This is due to lithium ion de-intercalate from LiFePO_4 and filled the negative electrode to reduce some of its irreversible capacity while during discharging the reversible lithium ion intercalate to LiFePO_4 peak was occur around 2.6V. This occupied process occurs at the electrode in this potential window which this desorption of anion in the voltage range of 4.2 V – 3.0 V and adsorption of lithium ion in the voltage range of 3.0 V – 2.2 V. By referring to the Figure 5, CD curve shows almost symmetry pattern for each cycle. The IR drop was not dramatic and promising capacity was always deliver by LICs.

Calculation of LIC energy density using Dr. Blade technique of coating shows that the specific capacitance is 237.62 F/g and the energy density as high as 74.6 Wh/kg. While the previous technique shows only 11.16 Wh/kg of their energy density, this technique is more effective with seven times higher value of the energy density. By comparison of the pre-doping method using Dr Blade technique, it will produce the most cycling stability and high performance of LIC.

4. CONCLUSION

The addition of 20% LiFePO_4 in the positive electrode of LIC, is the best proportion to add in positive electrode to obtain the best capacitance performance. The result leads to the increase in capacitance and contributes to the increase in the value of energy density. So, it is proposed that the pre-doping method will help to increase the capacitance of LIC. The level of lithium doping can be controlled by varying the amount of LiFePO_4 added to the positive electrode. The energy density obtained by Dr. Blade technique is 74.6 Wh/kg which is 7 times higher compared to the paste slurry in mesh. By using this technique, a very thin layer of electrode were produced, hence, lighter weight of electrode. This clearly shows that the pre-doping method using Dr. Blade technique can potentially produce the most stable cycle and the highest performance of LIC.

5. REFERENCES

1. S.R. Sivakumar, V.Ruiz, A.G Pondolfo Assembly and Testing of Lithium Ion Capacitors. 2010
2. G.G.Amatucci, F.Badway, A.D.Pasquier and T.Zheng. J.Electrochem. Soc. Vol. 148 (2001), p. A930
3. Khomenko V, Raymundo-Piñero E, Béguin F. High-energy density graphite capacitor in organic electrolyte. J Power Sources, 2008, 177:643–651
4. Overview of Lithium Ion Capacitor based system for compensation of short term power disruption.
5. Shi H, Barker J, Koksang R. Structure and lithium intercalation properties of synthetic and natural graphite. J Electrochem Soc, 1996,143: 3466–3472 Bose S, Kuila T
6. PING LiNa1, ZHENG JiaMing1, SHI ZhiQiang2*, QI Jie1& WANG ChengYang1* Electrochemical performance of MCMB/(AC+LiFePO4) lithium-ion capacitors chinese sc bulletin February 2013 Vol.58 No.6: 689-695
7. M.S.Park, Y.G.Lim, J.H.Kim, Y.J.Kim, J.Cho, J.S.Kim. A Novel Lithium Doping Approach for an Advance Lithium Ion Capacitor. Adv. Energy Mater. 2011, p 1002 -1006
8. F. Wu, H. Lu, Y. Su, S. Chen, Y. Guan. A Simple Way of Pre-doping Lithium Ion into Carbon Negative Electrode for Lithium Ion Capacitor. Material Science Forum Vol.650, 2010. P 142 – 149
9. N. Omar¹, J. Ronsmans², Yousef Firozu¹, Mohamed Abdel Monem¹, A. Samba, H. Gualous³, EVS27, Lithium-Ion Capacitor - Advanced Technology for Rechargeable Energy Storage Systems. Barcelona, November 17-20, 2013
10. V.Khomenko, E.Frackowiak, F.Beguin. Determination of the specific capacitance of conducting polymer/nanotubes composite electrode using different cell configurations. Vol 50, Issue 12 Pg 2499-2506, 2005
11. J.Gamby, Galvanostatic tests studies and characterisations of various activated carbon used for carbon/carbon supercapacitor. Journal of power sources 101(2001) 109-116
12. James. C. Ellenbogen, Marin S.Helper. Supercapacitor: A Brief Overview, 2006
13. Brunauer. S, Emmet P.H & Teller E. Adsorption of gasses in multimolecular layers. Journal of the American Chemical Society 60: 309-19. August 29, 1977

14. Signorelli.R, Kassakian J.G, Schindall J.E. Electrochemical Double-Layer Capacitors Using Carbon Nanotube Electrode Structures. Proceeding of IEEE. Vol 97 Issue 11 pg 1837-1847, 2009
15. V.Khomenko, E.Frackowiak, F.Beguin. Determination of the specific capacitance of conducting polymer/nanotubes composite electrode using different cell configurations. Vol 50, Issue 12 Pg 2499-2506, 2005
16. Merryl D. Stroller, Rodney S. Ruoff, Review of Best Practice for Determining an Electrode Material's Performance for Ultracapacitor, 2010
17. Bin Xu, Feng Wu, Renjie Chen, Gaoping Cao, Shi Chen, Guoqing Wang, Yushen Yang. Room Temperature molten salt as electrolyte for carbon nanotube-based electric double layer capacitors.

KAEDAH HIBRID FLIPPED CLASSROOM-PROBLEM BASED LEARNING : MENINGKATKAN KEMAHIRAN MENJAWAB SOALAN ARAS TINGGI

Marina Mokhtar

*Department of Applied Sciences, Universiti Teknologi MARA Cawangan Pulau Pinang, 13500 Permatang Pauh,
Penang, MALAYSIA.*

(E-mail: mmarina@ppinang.uitm.edu.my)

ABSTRAK - Kebolehan menjawab soalan peperiksaan dan ujian aras tinggi, memerlukan pengetahuan yang luas dan sentiasa mengikuti perkembangan isu semasa. *Basic Environmental Science* merupakan kursus asas persekitaran yang meliputi pengenalan kepada manusia, penempatan, atmosfera, air, tanah, bahan organik, kitaran biogeologi, masalah pencemaran dan penyelesaiannya. Oleh itu kaedah pengajaran secara tradisional tidak sesuai kerana ia hanya melibatkan komunikasi secara sehalu sahaja. Maka kaedah pengajaran hibrid *flipped classroom-problem based learning* (FC-PBL) telah dipraktikkan di dalam kelas sejak dua semester yang lalu. Objektif kajian ini adalah untuk melihat keberkesanan kaedah FC-PBL melalui perbandingan corak menjawab soalan aras tinggi di antara pelajar yang di ajar dengan kaedah tradisional dengan pelajar yang mengikuti kaedah FC-PBL. Melalui kaedah ini, pelajar dikehendaki untuk mengkaji isu semasa sebelum membincangkannya di dalam kelas. Pensyarah akan bertindak sebagai pemudah cara. Pendekatan ini di dapati telah meningkatkan pengetahuan am, kebolehan menganalisis dan mengeluarkan pendapat sendiri untuk menyelesaikan masalah yang berkaitan dengan masalah persekitaran.

Kata Kunci: Flipping classroom; Problem based learning; Berfikir aras tinggi; Kaedah pengajaran;

1. PENGENALAN

Soalan peperiksaan bukan sahaja meliputi soalan mudah dan sederhana tetapi juga soalan aras tinggi yang memerlukan kemahiran membuat analisis, menilai dan mengeluarkan pendapat sendiri. Kemahiran tersebut merupakan satu kebolehan yang perlu diasah selalu supaya boleh dikuasai sepenuhnya. Kursus *Basic Environmental Science* wajib diambil oleh pelajar Ijazah Sarjana Muda Kejuruteraan Kimia, merupakan satu kursus asas persekitaran yang meliputi pengenalan kepada manusia, penempatan, atmosfera, air, tanah, bahan organik, kitaran biogeokimia, masalah pencemaran dan penyelesaiannya. Seperti mana namanya, kursus ini sangat berkaitan dengan perubahan persekitaran dunia. Oleh itu, pengetahuan am dan isu semasa seseorang pelajar itu sangat penting bagi memastikan kualiti jawapan bagi soalan aras tinggi berada pada aras yang sangat baik.

Flipped classroom ialah satu konsep pedagogi yang menggantikan kuliah dalam kelas dengan peluang-peluang untuk meneroka dan mengkaji bahan-bahan yang di luar bilik darjah melalui klip video dan bacaan [1]. Sesi pembelajaran di dalam kelas akan menjadi satu proses yang aktif dengan gabungan (hibrid) kaedah pembelajaran berasaskan masalah (*problem based learning*). Rasional disebalik mengaplikasikan kaedah hibrid *flipped classroom – problem based learning* adalah pensyarah dapat menggunakan masa bersemuka (*face to face*) dengan membantu pelajar menguasai ilmu pengetahuan dengan lebih mendalam. Kertas kerja ini akan menerangkan latar belakang tentang kaedah *flipped classroom* yang dihibridkan dengan kaedah *problem based learning* serta tiga langkah pendekatan untuk menjayakan kaedah ini iaitu pelaksanaan, pengukuhan dan penilaian pedagogi ini.

Salah seorang pengamal terawal kaedah *flipped classroom* ialah Profesor Eric Mazur dari Universiti Havard. Beliau menyatakan bahawa kaedah tradisional iaitu perpindahan ilmu secara langsung di dalam kelas adalah tidak berkesan untuk membangunkan kebolehan pelajar untuk menggunakan ilmu yang diperolehi itu dengan berkesan [2]. Perkara ini sebenarnya adalah isu yang memang diketahui oleh penyelidikan sistem pendidikan di mana para pelajar tidak dapat menggunakan pengetahuan yang diperolehi untuk menyelesaikan masalah sebenar dalam kehidupan [3]. Secara pedagoginya, penyelesaian masalah ini perlulah berlandaskan kepada pembentukan persekitaran pembelajaran yang membolehkan pelajar berhadapan dengan situasi masalah sebenar yang mesti diselesaikan menggunakan ilmu pengetahuan yang diperolehi sebelum ini dari pensyarah mereka. Keadaan ini telah mendorong kaedah *flipped classroom* mencapai potensi yang baik di kalangan pendidik supaya pelajar memperoleh ilmu pengetahuan luar dari bilik darjah dan mengaplikasikannya ke atas masalah yang dikemukakan di dalam bilik darjah. Para pensyarah akan bertindak sebagai fasilitator dan penasihat. Kaedah pembelajaran berasaskan masalah (*problem based learning*) memerlukan seseorang pelajar itu untuk mengkaji, menghasilkan hipotesis, mengaplikasikan pengetahuan yang ada untuk menyelesaikan masalah yang diberikan [4]. Kerana itulah satu kaedah hibrid *flipped classroom- problem based learning* (FC-PBL) telah dibangunkan di dalam kajian ini. Kaedah *flipped classroom* ini menggalakkan pelajar untuk membuat ulangkaji ke atas material yang diberikan sebelum kelas bermula sebanyak yang mereka mahu [5]. Perkara penting seterusnya adalah pelajar akan dibantu apabila menganalisa maklumat daripada material tersebut [6]. Dalam keadaan ini, pelajar akan menjadi pelajar aktif yang menerima maklumbalas secara konsisten berdasarkan kepada tahap kefahaman mereka terhadap material yang diberikan [5].

Objektif kajian pelaksanaan kaedah FC-PBL ini dilakukan untuk menilai keberkesanan dalam meningkatkan kebolehan pelajar ijazah sarjana muda kejuruteraan kimia (persekitaran) menjawab soalan aras tinggi dengan kualiti yang lebih baik berbanding kaedah tradisional.

2. KAEDAH EKSPERIMEN

Penelitian telah dilakukan ke atas 30 orang pelajar yang mengikuti kursus *Basic Environmental Science* selama dua semester. Silibus kursus adalah sama bagi kedua-dua semester tetapi satu semester telah diajar dengan kaedah tradisional dan dianggap sebagai sampel rujukan, manakala satu semester lagi telah diajar dengan kaedah hibrid FC-PBL.

2.1 Pelaksanaan

Satu minggu sebelum kelas bermula, pelajar akan dibekalkan dengan artikel atau video pendek yang berkisarkan tentang isu persekitaran seperti pencemaran dan geologi yang berkaitan dengan tajuk yang akan disampaikan di dalam kelas. Medium penyampaian adalah melalui whatsapp kumpulan atau googlesite.

Pada waktu kelas, pelajar akan dibahagikan kepada beberapa kumpulan kecil. Setiap kumpulan akan mengenengahkan isu masing-masing beserta dengan jalan penyelesaiannya. Pensyarah akan menambahkan atau memberikan komen setiap cadangan yang diberikan supaya bersesuaian dengan pengajian pelajar iaitu seorang jurutera kimia persekitaran.

2.2 Pengukuhan

Untuk menilai keberkesanan kaedah FC-PBL ini, kumpulan pelajar tersebut perlu membangunkan satu video pendek berdurasi satu minit di luar bilik darjah dengan membincangkan isu persekitaran di sekitar kampus. Kami menamakan video ini sebagai “*One Minute Environmental Message*” yang mengandungi masalah sebenar serta cadangan jalan penyelesaiannya.

2.3 Penilaian

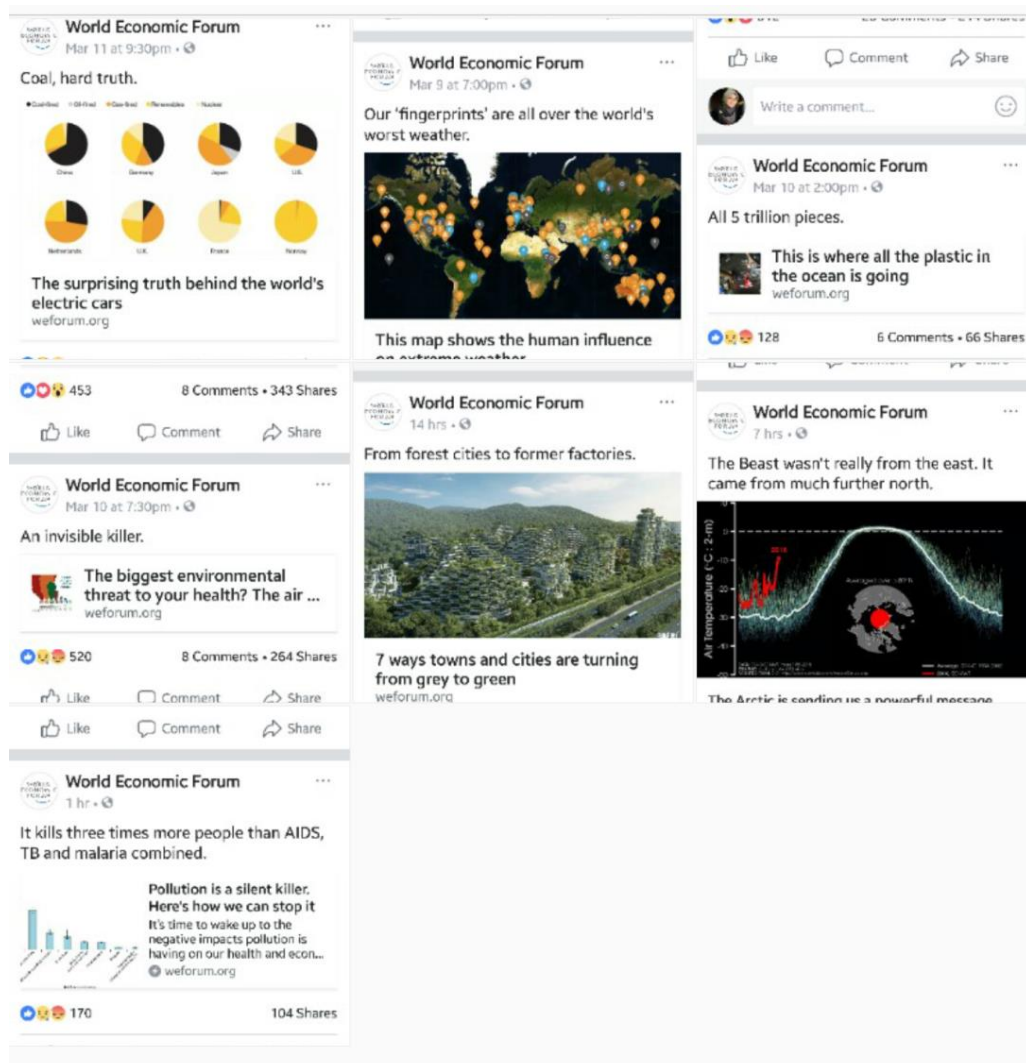
Para pelajar akan dinilai berdasarkan kebolehan menganalisa, menilai dan memberi cadangan penyelesaian di dalam soalan aras tinggi yang ditanya di dalam ujian dan peperiksaan Akhir.

3. KEPUTUSAN DAN PERBINCANGAN

3.1 Pemerhatian di dalam kelas

Pemerhatian yang dilakukan mendapati semua pelajar menjadi aktif semasa kelas sedang berlangsung. Mereka boleh mengajukan soalan kepada kumpulan yang sedang membentangkan isu mereka. Kumpulan pelajar yang membuat pembentangan juga dapat menguasai isu yang telah diberikan lebih awal itu, mengikut tahap kefahaman mereka. Pensyarah akan membantu meningkatkan kefahaman dan memberi komen terhadap cadangan penyelesaian yang dikemukakan.

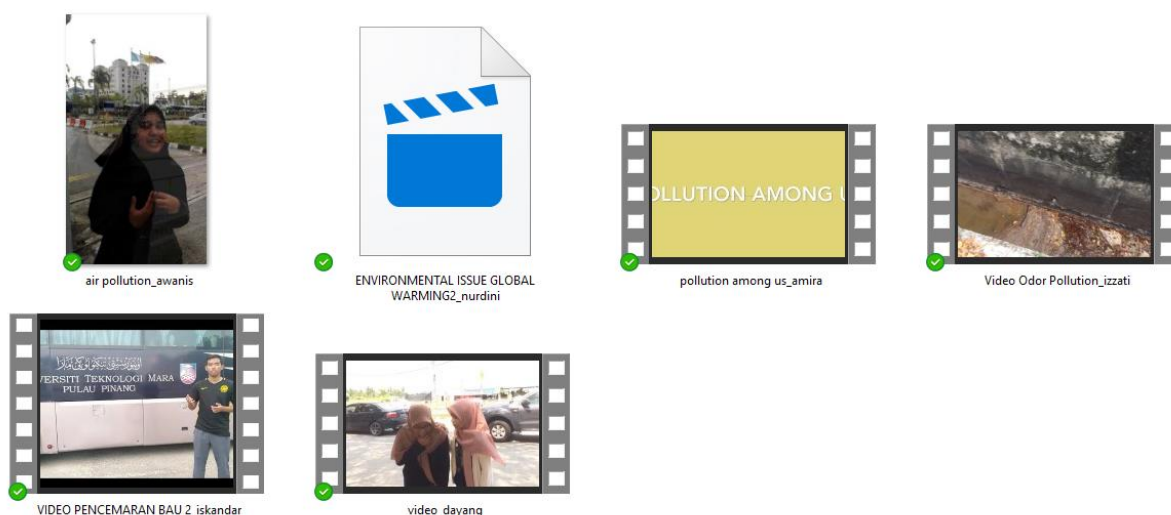
Para pelajar di dapati lebih bersedia memberikan jawapan atau respon terhadap contoh-contoh masalah yang ditanya di dalam kelas. Mereka telah mempunyai pengetahuan asas yang lebih baik sebelum menghadiri kelas. Contoh artikel mengenai masalah persekitaran adalah seperti yang ditunjukkan di dalam Rajah 1.



Rajah 1. Contoh artikel dan video pendek yang diberikan sebelum kelas bermula.

3.2 Pembuktian

Keberkesanan kaedah hibrid FC-PBL ini dibuktikan melalui kualiti jawapan terhadap soalan aras tinggi di dalam ujian dan peperiksaan akhir apabila dibandingkan dengan jawapan oleh pelajar yang telah mengikuti kaedah tradisional. Kaedah hibrid FC-PBL di dapati telah memantapkan pelajar dengan cara mereka berfikir untuk mengupas isu yang diberikan serta dapat mencadangkan jalan penyelesaian yang lebih teknikal bersesuaian dengan kerjaya yang bakal mereka ceburi iaitu jurutera kimia persekitaran. Rajah 2 menunjukkan video pendek “*One Minute Environmental Message*” yang dihasilkan oleh pelajar.



Rajah 2. Contoh video pendek yang telah dihasilkan oleh pelajar.

3.3 Perbandingan kaedah tradisional dengan kaedah hibrid FC-PBL

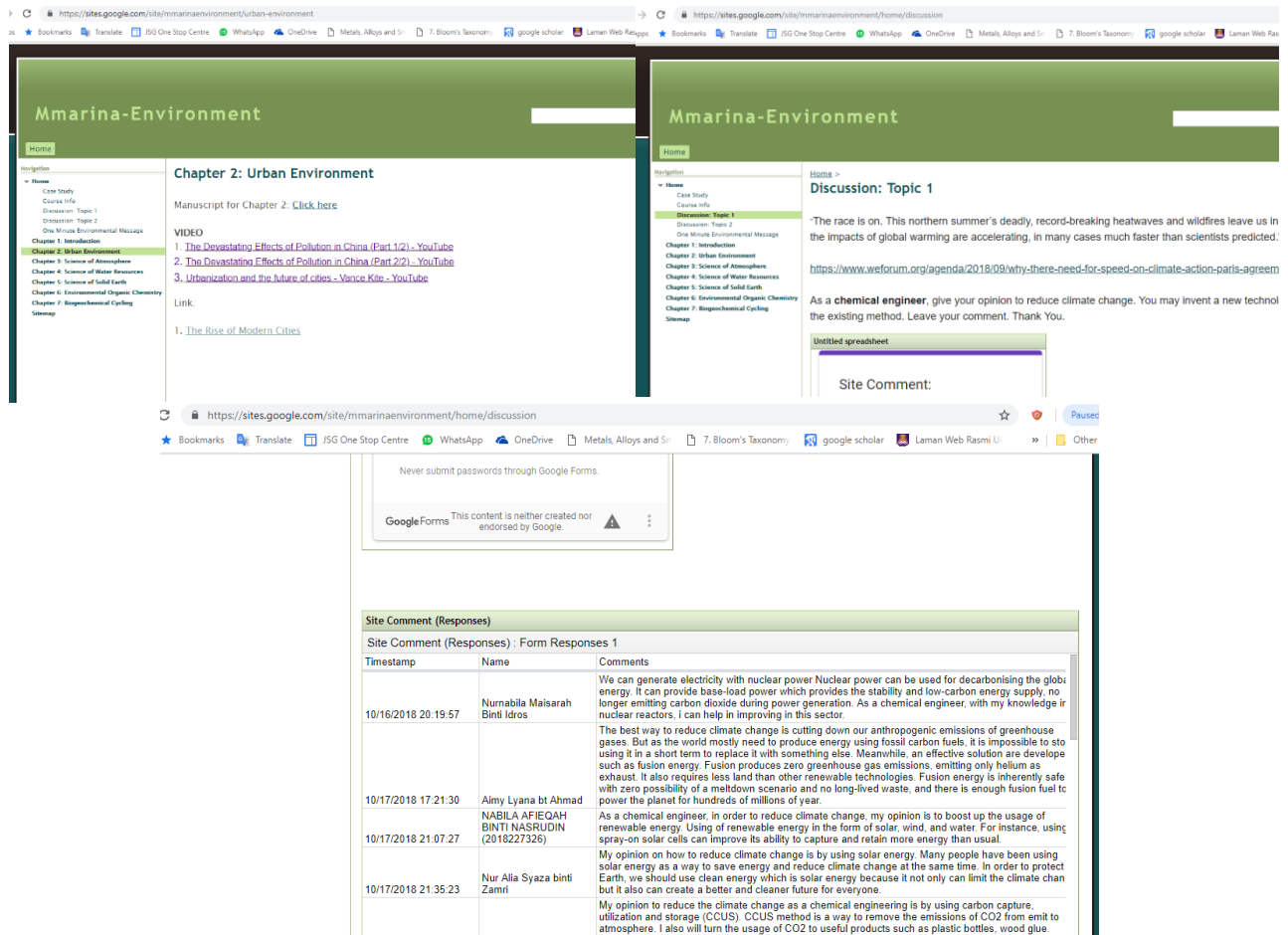
Ringkasan perbezaan pendekatan yang digunakan oleh kedua-dua kaedah ini adalah ditunjukkan seperti di dalam **Jadual 1**. Jadual ini jelas menunjukkan bahawa kaedah tradisional tidak menggalakkan pelajar membuat persediaan sebelum menghadiri kelas walaupun pelajar sering diingatkan untuk membuat bacaan dahulu sebelum hadir ke kelas.

Jadual 1. Perbandingan kaedah tradisional dengan hibrid FC-PBL

	Kaedah Tradisional	Kaedah hibrid FC-PBL
Sebelum kelas	-	Artikel masalah Video pendek
Semasa kelas	Syarahan	Pembelajaran Aktif
Selepas kelas	Tutorial menjawab soalan atau latihan.	Menghasilkan video pendek terhadap masalah sebenar di sekitar kampus.

Rajah 3 menunjukkan halaman googlesite sebagai salah satu medium menyampaikan material awal yang perlu dipelajari dahulu oleh pelajar. Googlesite sangat membantu pensyarah

dan pelajar kerana ia boleh menyediakan satu platform interaktif yang kekal dan sedia di akses di mana sahaja tanpa mengira masa.



Rajah 3. Medium googlesite sebagai perantara penyampaian material kepada pelajar.

Walaupun kaedah hibrid FC-PBL ini menuntut seseorang pelajar bekerja lebih tetapi impak yang bakal mereka perolehi adalah jauh lebih baik. Kaedah ini tidak membosankan kerana pelajar masa kini lebih suka kepada teknologi dan mudah mengikuti sesuatu pembelajaran melalui video pendek yang disertai dengan animasi. Strategi pembelajaran dengan kaedah *flipped classroom* atau kelas terbalik, dapat meminimumkan arahan dari pengajar. Kaedah ini juga dapat memanfaatkan teknologi yang dapat menyediakan material pembelajaran secara *online* dan mudah diakses oleh pelajar [7].

4. KESIMPULAN

Kaedah hibrid FC-PBL merupakan gabungan dua kaedah iaitu *flipped classroom* dan kaedah *problem based learning* yang telah meningkatkan kualiti dan cara menjawab soalan aras tinggi yang memerlukan seseorang pelajar itu untuk menganalisa masalah, menilai masalah dan mencadangkan jalan penyelesaian yang terkini dengan perkembangan semasa. Kaedah ini sememangnya sesuai untuk kursus *Basic Environmental Science* dan selari dengan wawasan universiti untuk menerapkan *Industrial Revolution 4.0* (IR 4.0) di dalam sistem pendidikan tinggi [8, 9].

5. RUJUKAN

1. Herreid, C.F. and N.A. Schiller, *Case studies and the flipped classroom*. Journal of College Science Teaching, 2013. 42(5): p. 62-66.
2. Mazur, E., *Farewell, lecture*. Science, 2009. 323(5910): p. 50-51.
3. Herrington, J. and R. Oliver, *An instructional design framework for authentic learning environments*. Educational technology research and development, 2000. 48(3): p. 23-48.
4. Savery, J.R., *Overview of problem-based learning: Definitions and distinctions*. Essential readings in problem-based learning: Exploring and extending the legacy of Howard S. Barrows, 2015. 9: p. 5-15.
5. Bishop, J.L. and M.A. Verleger. *The flipped classroom: A survey of the research*. in *ASEE national conference proceedings, Atlanta, GA*. 2013.
6. Fautch, J.M., *The flipped classroom for teaching organic chemistry in small classes: is it effective?* Chemistry Education Research and Practice, 2015. 16(1): p. 179-186.
7. Rahayu, L.P. *Efektivitas Strategi Pembelajaran Flipped Classroom pada Materi Pythagoras SMP Kelas VIII Ditinjau Berdasarkan Gender*. in *Prosiding SI MaNIs (Seminar Nasional Integrasi Matematika dan Nilai-Nilai Islami)*. 2017.
8. Xing, B. and T. Marwala, *Implications of the Fourth Industrial Age on Higher Education*. arXiv preprint arXiv:1703.09643, 2017.
9. Brown-Martin, G. *Education and the Fourth Industrial Revolution 2017*; Available from: <https://medium.com/learning-re-imagined/education-and-the-fourth-industrial-revolution-cd6bcd7256a3>.

HYDROTHERMAL SYNTHESIS OF FE DOPED SnO₂ NANORODS FOR ETHANOL GAS SENSOR.Vicinisvarri Inderan^{1,2,a}, Kumar Sudesh^{3,b}, Hooi Ling Lee^{2,c,*}¹*Department of Applied Sciences, Universiti Teknologi MARA Cawangan Pulau Pinang, 13500 Permatang Pauh, Penang, MALAYSIA.*²*Nanomaterials Research Group, School of Chemical Sciences, Universiti Sains Malaysia, 11800 Minden, Penang, Malaysia*³*School of Biological Sciences, Universiti Sains Malaysia, 11800 Minden, Penang, Malaysia.*(E-mail: ^avicinisvarri@ppinang.uitm.edu.my, ^bksudesh@usm.my, ^chllee@usm.my)

ABSTRACT - In most metal oxide based gas sensor applications, doping with transition metal is a widely used approach in order to improve the gas sensing properties of sensor materials. In this work, undoped SnO₂ and Fe doped SnO₂ nanorods were successfully synthesized *via* hydrothermal method at a relatively low temperature, 180 °C without organic templates, surfactants or further calcination. X-ray diffraction (XRD) analysis confirmed that both undoped SnO₂ and Fe doped SnO₂ powder samples were consisting of rutile tetragonal phase SnO₂. There were no peaks of other impurities such as metallic tin (Sn), stannous oxide (SnO), ferrous oxide (FeO) and ferric oxide (Fe₂O₃) were detected. High resolution transmission electron microscopy (HRTEM) analysis revealed that the average diameter and length of nanorods formed in Fe doped SnO₂ sample were approximately 4 and 32 nm than the nanorods formed in undoped SnO₂ (25 and 150 nm), respectively. Subsequently, the aspect ratio of Fe doped SnO₂ increased (aspect ratio, 8) compare to that of undoped SnO₂ (aspect ratio, 6). A simple ethanol gas sensing test was carried out at 450 °C using 1000 ppm ethanol gas. The Fe doped SnO₂ nanorods sensor recorded almost similar sensing response reading (1.4×10^3) than that of undoped SnO₂ nanorods, 1.1×10^3 although the size of nanorods Fe doped SnO₂ decreased drastically. However, the initial resistance of Fe doped SnO₂ nanorods far higher than undoped SnO₂.

Keywords: Hydrothermal, tin oxide, Fe doped, ethanol gas sensor.

1. INTRODUCTION

The doping of tin oxide gas sensor is one of the traditional approaches used to enhance the gas sensitivity, selectivity and decrease the operating temperature. So far, various dopants including noble metals, transition metals, non-metals, alkaline earth metals and metalloid can be used. Among them, noble metals (Pd, Pt, Au, Ag, Rh) and transition metals (e.g Fe, Co, Cu, Ni, etc.) are the most common metals used as dopants in gas sensor applications. Generally, noble metal dopants serve as “catalyst” whereas transition metal dopants serve as “accelerator” of various process [1]. Ferum (Fe) is a ferromagnetic metal belongs to Group 8 in the periodic table. Generally, it was reported the incorporation of Fe dopant in semiconducting metal oxide appears in the form of Fe³⁺ which highly influenced the band gap and electrical properties of gas sensor [2]. Although there are several reports available in the literatures about the structural and magnetic properties of Fe doped SnO₂ nanostructures, the reports on the Fe doped SnO₂ as gas sensor are quite limited [3-6]. Meanwhile, the one-dimensional (1-D) metal oxide nanostructures are found to be very promising for gas sensor applications due to the surface to volume ratio is very high and which subsequently improve the sensor sensitivity [7]. A number of methods such as thermal evaporation [8], hydrothermal [9], chemical vapor deposition (CVD) [10], sol-gel [11] and co-precipitation [12] have been employed to synthesis 1-D SnO₂ nanostructures. Among them, hydrothermal route is considered as a promising method widely used to synthesis

homogeneous SnO₂ nanostructures with controlled shape and size. Herein, in this study we prepared 1-D undoped and Fe doped SnO₂ nanorods via hydrothermal method using neither organic template nor surfactant at a relatively low temperature, 180 °C. The as-synthesized SnO₂ nanorods samples were then tested on 1000 ppm ethanol gas at 450 °C. The morphological and structural properties of as-synthesized SnO₂ were investigated using X-ray powder diffraction (XRD) and high-resolution transmission electron microscopy (HRTEM) analysis.

2. EXPERIMENTAL METHOD

The hydrothermal method was executed to synthesis undoped and Fe doped SnO₂ nanorods samples depicted in Figure 1.

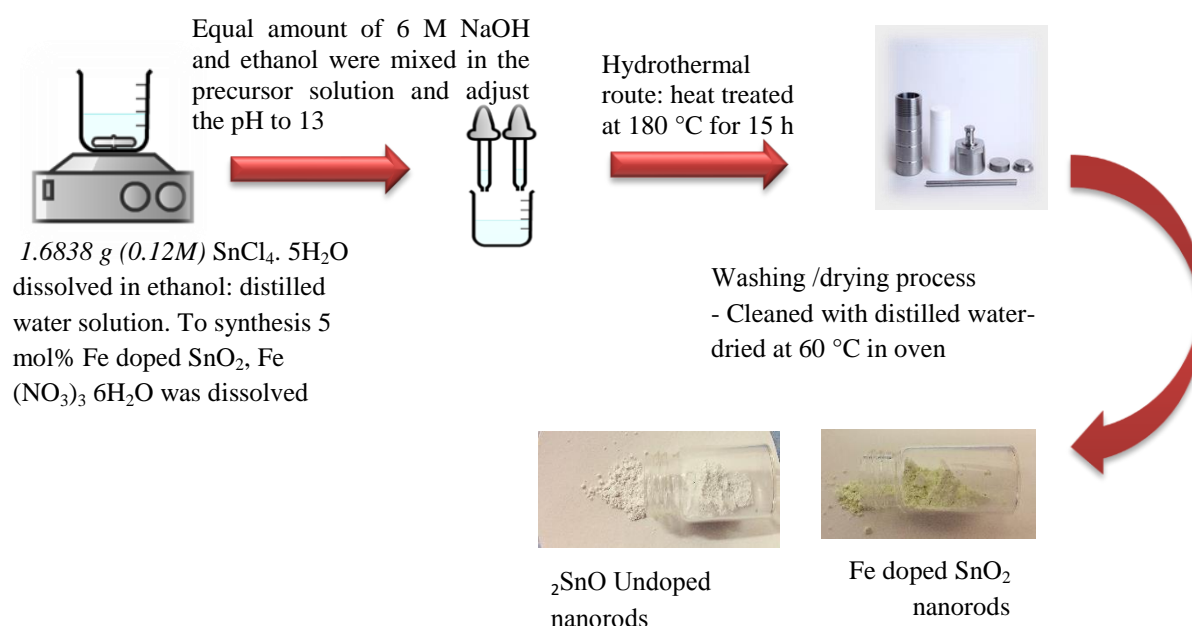


Figure 1. The hydrothermal synthesis of undoped and Fe doped SnO₂ nanorods.

3. RESULTS AND DISCUSSION

Table 1 shows the XRD data obtained for undoped and Fe doped SnO₂ nanorods powder samples. nanorods, respectively.

Table 1. The calculated crystalline sizes, lattice constants and lattice strains of undoped and Fe doped SnO₂ nanorods powder samples.

Sample	Crystalline (size (nm	Lattice strain	Lattice constant, a	Lattice constant, c
₂ Undoped SnO	32.00	0.0038	4.7098	3.1751
₂ Fe doped SnO	12.90	0.0096	4.7343	3.1781

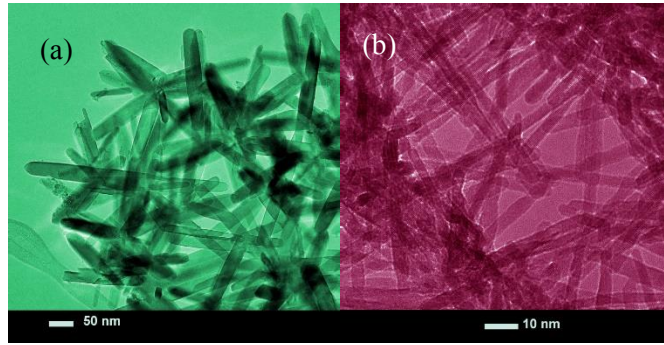


FIGURE 2: HRTEM micrographs of (a) undoped SnO₂ nanorods (b) Fe doped SnO₂, respectively.

The HRTEM micrographs in Figure 2 exhibits the morphology of (a) undoped and (b) Fe doped SnO₂ nanorods, respectively. The average diameter and length of undoped SnO₂ nanorods were 2 nm and 150 nm, respectively. After doped with Fe, the average diameter and length reduced to 4 nm and 32 nm. Figure 3 displays the ethanol gas sensing response of undoped and Fe doped SnO₂ nanorods sensor. It is noteworthy that the initial resistance of Fe doped SnO₂ nanorods sensor higher than that undoped SnO₂. This can be explained due o the smaller size of nanorods (diameter ~4 nm) increased the thickness of charge depletion layer subsequently increases the initial resistance. Interestingly, the Fe doped SnO₂ nanorods sensor recorded almost similar response with undoped SnO₂, 1.4×10^3 and 1.1×10^3 respectively. This result similiar to the previous study [6]. The recovery time of Fe doped SnO₂ also improved.

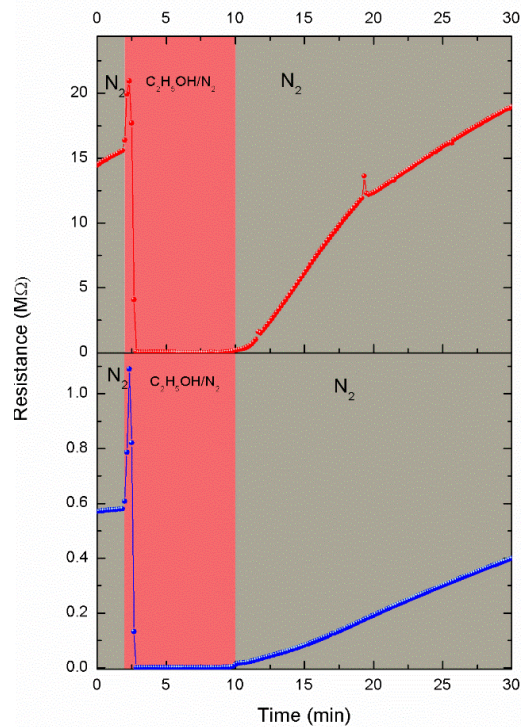


Figure 3 The resistance of (a) Fe doped SnO₂ and (b) undoped SnO₂ nanorods sensor at 450 °C.

4. CONCLUSION

The 1-D undoped and Fe doped SnO₂ nanorods were successfully synthesized using hydrothermal method. The average diameter and length of Fe doped SnO₂ nanorods reduced to 4 nm and 32 nm, respectively. However, the aspect ratio increased from 6 to 8 after Fe doping. The ethanol gas sensing response of Fe doped SnO₂ at 450 °C found to be almost similar to the undoped SnO₂ nanorods sensor although the initial resistance of Fe doped SnO₂ far higher than that of undoped SnO₂. It is suggested that the smaller size of nanorods responsible of the high initial resistance reading.

5. REFERENCES

1. G. S. (Gennadii S. Korotchenkov, *Handbook of gas sensor materials : properties, advantages and shortcomings for applications. Volume 2, New trends and technologies.* 2013.
2. J. J. Beltrán, C. A. Barrero, and A. Punnoose, "Understanding the role of iron in the magnetism of Fe doped ZnO nanoparticles.," *Phys. Chem. Chem. Phys.*, vol. 17, no. 23, pp. 15284–96, Jun. 2015.
3. V. Vaishampayan, R. G. Deshmukh, P. Walke, and I. S. Mulla, "Fe-doped SnO₂ nanomaterial: A low temperature hydrogen sulfide gas sensor," *Mater. Chem. Phys.*, vol. 109, no. 2–3, pp. 230–234, 2008.
4. K. Galatsis *et al.*, "p-and n-type Fe-doped SnO₂ gas sensors fabricated by the mechanochemical processing technique," *Sensors Actuators B*, vol. 93, no. 1, pp. 562–565, 2003.
5. R. Xu *et al.*, "One-step synthesis and the enhanced xylene- sensing properties of Fe-doped MoO₃ nanobelts," *RSC Adv.*, vol. 6, no. 108, pp. 106364–106369, 2016.
6. A. Khayatian, S. Safa, R. Azimirad, M. A. Kashi, and S. F. Akhtarianfar, "The effect of fe-dopant concentration on ethanol gas sensing properties of fe doped ZnO/ZnO shell/core nanorods," *Phys. E Low-dimensional Syst. Nanostructures*, vol. 84, pp. 71–78, Oct. 2016.
7. Pal, M. Pal, and R. S. Zeferino, "Gram-scale synthesis of highly crystalline, 0-D and 1-D SnO₂ nanostructures through surfactant-free hydrothermal process," *J. Nanoparticle Res.*, vol. 14, no. 7, p. 969, Jun. 2012.
8. S. H. Luo *et al.*, "Vacuum electron field emission from SnO₂ nanowhiskers synthesized by thermal evaporation," *Nanotechnology*, vol. 15, no. 11, pp. 1424–1427, Nov. 2004.
9. S. Nasresfahani, M. H. Sheikhi, M. Tohidi, and A. Zarifkar, "Methane gas sensing properties of Pd-doped SnO₂ / reduced graphene oxide synthesized by a facile hydrothermal route," *Mater. Res. Bull.*, vol. 89, pp. 161–169, 2017.
10. M. Kwoka, L. Ottaviano, M. Passacantando, S. Santucci, G. Czempik, and J. Szuber, "XPS study of the surface chemistry of L-CVD SnO₂ thin films after oxidation," *Thin Solid Films*, vol. 490, no. 1, pp. 36–42, Oct. 2005.
11. A. V. Marikutsa, M. N. Rumyantseva, L. V. Yashina, and A. M. Gaskov, "Role of surface hydroxyl groups in promoting room temperature CO sensing by Pd-modified nanocrystalline SnO₂," *J. Solid State Chem.*, vol. 183, no. 10, pp. 2389–2399, 2010.
12. Maolin Zhang, Guoying Sheng, Jiamo Fu, Taicheng An, Xinming Wang, and Xiaohong Hu, "Novel preparation of nanosized ZnO–SnO₂ with high photocatalytic activity by homogeneous co-precipitation method," *Mater. Lett.*, vol. 59, no. 28, pp. 3641–3644, Dec. 2005.

STRUCTURAL AND OPTICAL CHARACTERIZATION OF POROUS ZINC OXIDE (ZnO) GROWN ON DIFFERENT SUBSTRATES BY AMMONIUM HYDROXIDE (NH₄OH) SOLUTION

Mohd Zaki Mohd Yusof¹, Nur Hazwani Abu², Mohd Muzafa Jumidali¹, Mohd Bukhari Md Yunus¹, Muhammad Firdaus Othman¹

¹ *Department of Applied Sciences, Universiti Teknologi Mara kampus Permatang Pauh, Penang, Malaysia*

² *Faculty of Chemical Engineering, Universiti Teknologi Mara kampus Permatang Pauh, Penang, Malaysia*

(E-mail: zaki7231@ppinang.uitm.edu.my)

ABSTRACT-The present study reports the growth and characterization of the fabrication of porous ZnO on different substrate. Porous zinc oxide is a favorable material for various applications and it can be fabricated by wet chemical etching on the different substrates. The ZnO thin films was deposited using radio frequency (RF) sputtering method on silicon, glass, sapphire and PET substrates. The ZnO thin films was etched in the ammonium hydroxide (NH₄OH) solution for 3 minutes to form porous ZnO thin films. The Optical Microscopy, Filmetrics and Fourier Transform Infrared Spectroscopy (FTIR) results have been analyzed to determine the surface morphology, refractive index and functional group correspondingly grown on different substrate which is glass, silicon, sapphire and PET substrate. The FTIR revealed that there is ZnO bond that exist on the ZnO/silicon samples and the optical microscope show that there is better formation of pores on the ZnO/silicon samples. However, for the filmetrics it shows the decreasing of reflectance due to the porosity on ZnO/silicon. The refractive index that has been obtained are 0.9301 and 0.9667 for ZnO and porous ZnO porous respectively. Meanwhile, the thickness that obtained are 365.3 Å for ZnO and 262.6 Å for porous ZnO. Finally, silicon substrate was a better substrate for the fabricating porous ZnO using ammonium hydroxide (NH₄OH) solution.

Keywords: Zinc Oxide, Porous ZnO, Ammonium Hydroxide, Wet Chemical Etching.

1. INTRODUCTION

Zinc oxide can be known as a multifunctional material on account of its distinctive physical and compound properties [3]. ZnO nanomaterials have been widely considered for application in different sorts of nanoscale useful gadgets utilized generally as a part of the chemical industry, medical diagnostics, food technology, ultraviolet testing, national barrier and our daily life [4]. There are a few strategies to forming and manufacture the ZnO nanostructures on different substrate including chemical vapor deposition (CVD), pulsed laser deposition, spray pyrolysis and radio frequency (RF) magnetron frequency and many others[5].

The fabrication of porous and nanostructured ZnO is a different focus of interest due of the competence of this material to modify ZnO optical properties that are suitable for device fabrication, especially for optoelectronic devices [6]. In contrast, the researchers has taken an interest in porous ZnO for its large internal surface area. Wet chemical etching is a reliable method for producing porous materials. This method involves a few controlling parameters and is relatively cost-efficient [6]. Some studies by other researchers on fabrication of porous ZnO

focus on some methods such as electrodeposition, chemical etching, unbalanced magnetron sputtering, electrochemical anodization has been proved.

Lately, the difference in the etching solution and substrate is so far to be recognized for the porous ZnO formation. Henceforward, the formation of porous ZnO need to be discover further using an etching solution on different substrate such as glass, silicon, sapphire and PET substrate [6]. It has been proven by the C.G.Ching et al, (2013) and S.S.Ng et al, (2014) that fabricated porous ZnO on the silicon substrate using electrochemical etching solution was the latest one.

2. EXPERIMENTAL DETAILS

For the preparation of the sample, the sample was cleaned using the RCA method cleaning process. The ZnO thin films was deposited on different substrate by using RF sputtering method. The power of the RF sputtering was set at 150W and at room temperature. The Argon gas was used as a spectral gas and vacuum chamber evacuated base pressure at 3.49×10^{-5} mbar. The substrate was pre-sputtered for about 10 minutes to make sure there was no contamination to the surface of the substrate. Then, the porous ZnO was prepared by wet etching. The ZnO films of different substrate were etched using 100 ml NH_4OH solution with the etching time of 3 minutes. After the etching process, the samples were rinsed with distilled water and dried under nitrogen gas flow to remove any chemical residue on the sample surface. In this experiment, the etching time use is for 3 minutes. For a better and accurate result, the various etching time such as between 1 minutes to 5 minutes need to be observed to get the average [31]. The characterization methods used are Optical Microscopy, Fourier Transform Infrared Spectroscopy (FTIR) and Filmetrics. In this experiment, the analysis used was Optical Microscopy, Fourier Transform Infrared Spectroscopy (FTIR) and Filmetrics. For a better observation, other analysis such as SEM, XRD and PL Spectra also need to be considered [38].

3. RESULTS AND DISCUSSION

Figure 1(a)-(h) shows the surface morphology of the ZnO thin film grown on the different substrate before and after etched with 100 ml ammonium hydroxide (NH_4OH) solution at 3 min of etching times respectively. The image before etched with 100 ml ammonium hydroxide (NH_4OH) solution shows that the surface morphology of the ZnO thin film has an irregular shaped structure for all the different substrates. After immersing in the ammonium hydroxide (NH_4OH) solution, the pores initially formed on the ZnO surface of the different substrates. Overall, the surface morphologies of the porous ZnO after etched on sapphire substrate show the smoother surface among the glass, silicon and PET substrates. Figure 1(g) and (h) show that there are numerous formation of pores on silicon substrate compared to the other substrates. This is because the silicon substrate has the tendency to contain a higher degree of dislocation because of the relatively large lattice mismatch between ZnO and Si substrate [6]. It has proven that silicon substrate is the most suitable substrate to etched in ammonium hydroxide (NH_4OH) solution compared to the other substrate. Furthermore, among the four substrates, the PET substrate is the mostly not suitable to etched in ammonium hydroxide (NH_4OH) solution.

Beside that, there are maybe because of some factors that make the pores size formation different on the different substrates[10]. The variation in the morphology of the obtained porous ZnO is attributed to the active dissolution of grains ZnO in NH_4OH solution. The etching process is believed to initiate at the defect sites on the ZnO film, namely, the edge of the grains ZnO, as soon as it was exposed to the NH_4OH solution [7].

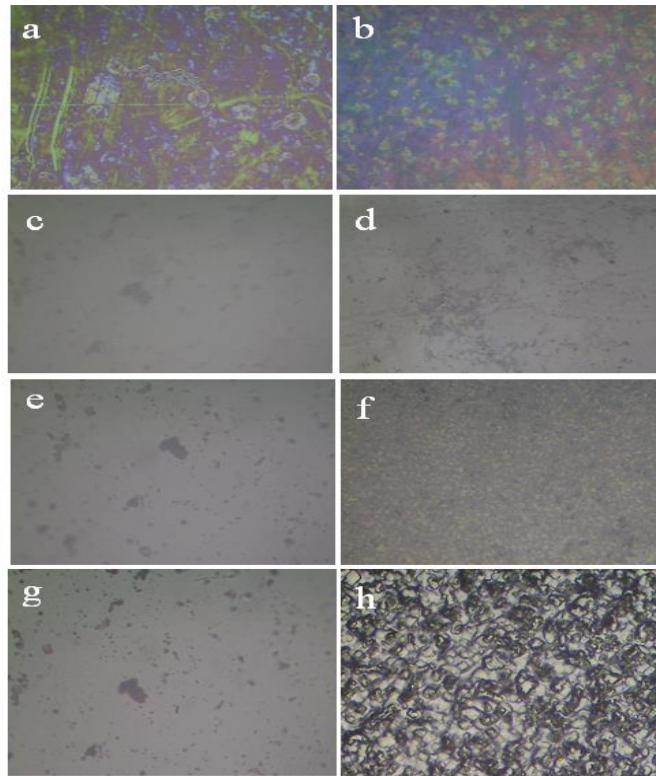


Figure 1. Surface morphology for thin film of ZnO grown on (a),(b) glass, (c),(d) PET, (e),(f) sapphire and (g),(f) silicon substrate (a),(c),(d),(e) before and (b),(d),(f),(h) after etched in ammonium hydroxide (NH_4OH) solution.

Figure 3 shows the filmetrics result for thin film of ZnO grown on silicon substrate before (ZnO) and after (porous ZnO) etched in ammonium hydroxide (NH_4OH) solution. The silicon substrate was further investigated to the filmetrics analysis because it is the most suitable substrate as mentioned in the optical microscopy analysis and FTIR analysis before. From the filmetrics analysis, the refractive index that has been analyzed are 0.9301 and 0.9667 for ZnO and porous ZnO respectively. Meanwhile, the thickness that obtained are 365.3 \AA for Si control and 262.6 \AA for Si porous. Reflectance is the fraction of the total radiant flux incident upon a surface that is reflected and that varies according to the wavelength distribution of the incident radiation. From the graph that has been plotted, it can be concluded that there is a decrease after the ZnO thin film was etched in the ammonium hydroxide (NH_4OH) solution. This happened due to the surface roughness and the pores that formed on the surface of the silicon substrate. Therefore, the refractive index decreased and was controlled by the pores with respect to the high porosity which consequently led to a decrease in reflection [12].

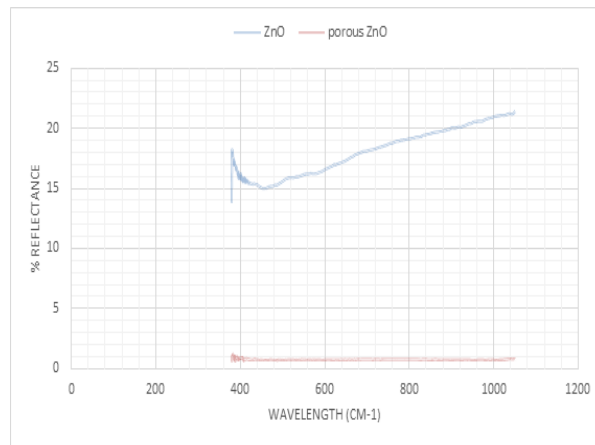


Figure 3. Filmetrics result for thin film of ZnO grown on silicon substrate before and after etched in ammonium hydroxide (NH₄OH) solution.

4. CONCLUSION

Throughout the experiment that has been conducted, it can be concluded that ZnO has many unique properties that can be applied in the electronic field. The thin film of ZnO was deposited using the reactive sputtering system which is Auto HHV500 Sputter Coater model. The ZnO thin films on the different substrate which is glass, sapphire, silicon and PET substrate was etched into the ammonium hydroxide (NH₄OH) solution for about 3 minutes of the etching time for porous ZnO thin films. After that, the porous ZnO thin films was analyzed to observed their surface morphology and the functional group using Optical Microscopy and Fourier Transform Infrared Spectroscopy (FTIR) respectively. Besides that, the thickness and their refractive index was determined using the Filmetrics F20 analysis. It can be conclude that, for the Optical Microscopy Analysis, there are better formation of pores on the silicon substrates compared to other substrate. So, it was further investigation to determined the effects of reflectance before and after etched in the ammonium hydroxide (NH₄OH) solution using Filmetrics F20 analysis. The reflectance was decrease after the ZnO thin films was etched in the NH₄OH solution. The ZnO bonds was found less than 500 cm⁻¹ on the graph of absorbance versus wavelength for the silicon substrate. Lastly, it has been proven that, silicon substrate was a better substrate for the wet chemical etching using ammonium hydroxide (NH₄OH) solution.

5. ACKNOWLEDGEMENTS

The authors would like to express gratitude for the support given by the Universiti Teknologi Mara.

6. REFERENCES

- [1] A. Janotti and C. G. Van De Walle, "Fundamentals of zinc oxide as a semiconductor," vol. 72, 2009.
- [2] T. Analyzer, "Filmetrics F20 Manual," *Film. Inc.*, 2007.
- [3] A. Kołodziejczak-radzimska and T. Jesionowski, "Zinc Oxide—From Synthesis to Application: A Review," pp. 2833–2881, 2014.
- [4] D. Hofstetter and H. Morkoc, "ZnO Devices and Applications : A Review of Current Status and Future Prospects," no. 7, pp. 1255–1268, 2010.

- [5] R. S. Gonçalves, P. Barrozo, and F. Cunha, "Optical and structural properties of ZnO thin films grown by magnetron sputtering: Effect of the radio frequency power," *Thin Solid Films*, vol. 616, pp. 265–269, 2016.
- [6] Z. H. & H. A. H. C.G.Ching, Leonard I., C.I. Angg, P.K. Ooi, S.S. Ng, "Effects of the Nitric Acid Concentrations on the Etching Process , Structural and Optical Properties of Porous Zinc Oxide Thin Films," vol. 42, no. 9, pp. 1327–1332, 2013.
- [7] H. Abu. Hassan. & Z. Hassan. S.S. NG, P.K. OOI, S. Yaakob, M.J. Abdullah, "Fabrication of Porous ZnO Thin Films via Ammonium Hydroxide : Effects of Etching Time and Oxidizer on Surface Morphology and Surface Roughness," vol. 43, no. 7, pp. 1077–1082, 2014.
- [8] H. Z. Moussambi, H. Gnanga, A. Giani, and A. Foucaran, "Optical properties of ZnO thin films deposited by RF magnetron," vol. 10, no. 29, pp. 173–181, 2015.
- [9] C. Shang, Y. Thimont, A. Barnabé, L. Presmanes, I. Pasquet, and P. Tailhades, "Detailed microstructure analysis of as-deposited and etched porous ZnO films," *Appl. Surf. Sci.*, vol. 344, pp. 242–248, 2015.
- [10] K. Carlsson, "Light Microscopy," *Phys. Biomed.*, p. 75, 2007.
- [11] H.-C. Lu, "Porous Materials," *J. Porous Mater.*, vol. 53, no. 619, pp. 743–747, 2012
- [12] K. A. Salman, "Growth of Zinc Oxide Nanocombs on Porous Silicon Layer by Thermal-Evaporation Method," *Adv. Mater.*, vol. 4, no. 2, p. 30, 2015.

FABRICATION AND CHARACTERIZATION OF ZINC OXIDE (ZnO) THIN FILMS ON GLASS SUBSTRATE BY RADIO FREQUENCY (RF) SPUTTERING TECHNIQUE

Mohd Muzafa Jumidali¹, Siti Amira Norafarih An Ismoni², Mohd Zaki Mohd Yusoff¹, Mohd Bukhari Md Yunus¹, Muhammad Firdaus Othman¹

¹Department of Applied Sciences, Universiti Teknologi Mara kampus Permatang Pauh, Penang, Malaysia

²Faculty of Chemical Engineering, Universiti Teknologi Mara kampus Permatang Pauh, Penang, Malaysia

(E-mail: mohdmuza433@ppinang.uitm.edu.my)

ABSTRACT- The ZnO is popular in the research fields nowadays because it novel properties which attracted various applications to use it. There is various types of method were used to deposit the ZnO thin film. However, not all the method will produce the high quality of thin film because of it limitations. In this research, the RF sputtering method was chosen because the method has some advantages compared to the other methods. The project was conducted to fabricate the ZnO thin film on the glass substrate by using RF sputtering, and to anneal and characterize the ZnO thin films on a glass substrate at different temperature by using Filmetric, FTIR, and optical microscope. ZnO thin films were deposited on the glass substrate by RF sputtering and then, the ZnO thin films were annealed at different temperatures; 200°C, 300°C, and 400°C in tube furnace for one hour. The optical property and surface morphology of annealed ZnO thin films were characterized. The refractive index of the ZnO thin film, the measurements were decreased when the higher annealing temperature was used which is from 1.6153 (200 °C), 1.4154 (300 °C) and 1.3541(400 °C). In addition, the higher transmittance was observed which is greater than 70%, and the absorbance shows that the four sample contain ZnO as the peak at range of 420.431 cm⁻¹ to 450.30 cm⁻¹ were presented which represent ZnO stretching and the present of O-H groups at range 3568.233 cm⁻¹ to 3628.15 cm⁻¹ shows the hygroscopic nature of ZnO. The surface morphology of the thin films were increased as the annealing temperature increased where the surface roughness was reduced and become smoother as the annealed temperature increased at above 200°C.

Keywords: Zinc Oxide, Porous ZnO, Ammonium Hydroxide, Wet Chemical Etching.

1. INTRODUCTION

Nowadays, Zinc Oxide (ZnO) is one of an attractive material that is used for research due to its performance in optics, photonics and electronics. There are many application that used ZnO material such as UV light-emitters, varistors, transparent high power electronics, surface acoustic wave devices, piezo-electric transducers, gas-sensing and as a window material for display and solar cells [1]. ZnO is a semiconductor that at a room temperature have a wide direct band gap energy which is approximately to 3.37 eV and a large exciton binding energy that approximately 60mV [2]. At a room temperature, the high exciton binding energy can ensure effective excitonic emission in ZnO [3]. In addition, the wide direct band gap energy in ZnO can let the devices to operate at high temperature and enable the ZnO to be transparent where in the visible spectrum, it brings the electronic transition energy into the energy range of visible light [4,5]. This shows

that ZnO semiconductor have several properties such as high electron mobility, good transparency and high durability of room temperature luminescence. There are many techniques that had been used for growing the ZnO as a thin films on the various substrates such as chemical spray pyrolysis [6], successive ionic layer adsorption and reaction (SILAR) [7], pulsed laser deposition technique (PLD) [8] and radio frequency sputtering [9]. These methods have their own advantages and disadvantages such as in chemical spray pyrolysis, this method has advantages such as it does not require high quality of target, easy to control of composition and microstructure and can be conducted at moderate temperature at the range of 100°C to 500°C but these methods also have limitations such as the spray nozzle may become cluttered after long processing time and the quality of films depends on the size of the droplet and spray nozzle [10]. When the quality of film produced by chemical spray pyrolysis depends on the size of the droplet and spray nozzle, it shows that the deficiency of the method could be occurred during the film deposition which tends to produce low quality of thin film. That means not all techniques are suitable to produce high quality of ZnO thin film. In this research, radio frequency sputtering method was chosen to fabricate the ZnO thin film on glass substrate because the RF sputtering method is a simple method to fabricate the ZnO thin films and it has better control on the film growth, required low temperature deposition, and uniform film properties [11]. Soda lime glass substrate was chosen to deposit the ZnO thin films because it has higher resistance to high temperature, high transmission, brittle, and inexpensive. However, there are some disadvantages of soda lime glass where it is easily cracked when heated and cooled since the soda lime glass has high thermal expansion, and it cannot be used in strong acids and alkalis [12]. After deposition, the ZnO thin films were annealed in order to improve the surface morphology of the thin films where the crystallite size of the thin film increased and the surface roughness of the film decreased. According to Tuzemen et al., 2013 [13], the optimal temperature of annealing is at high temperature which is at the range between 350°C and 500°C because it was reported that at this range of the annealed temperature, the surface morphology of the ZnO thin films were increased. In this research, the objectives are to fabricate the ZnO thin film on the glass substrate by using RF sputtering, and to anneal and characterize the ZnO thin films on a glass substrate at different temperatures by using Filmetric, FTIR, and optical microscope. The zinc oxide thin film was fabricated on glass substrate by using radio frequency sputtering technique. Then, the ZnO thin film on the glass substrate will be annealed at different temperatures by thermal tube furnace. The annealed films at different temperatures then will be characterized by Filmetric, Fourier Transform Infrared Spectroscopy (FTIR), and optical microscope in terms of optical properties and surface morphology.

2. EXPERIMENTAL DETAILS

Zinc oxide films were deposited on glass substrate by RF sputtering technique using a zinc oxide target (99.99%). The substrates were ultrasonically cleaned in deionized water for 15 minutes and dried using dry nitrogen. Then, the ZnO thin films were deposited by using RF sputtering method. The RF power was kept constant at 150W and the temperature of the substrate was set to room temperature. The vacuum chamber was evacuated to a base pressure of 3.54×10^{-3} mbar and Argon gas was introduced into the chamber. The pre-sputtering was conducted for 10 minutes in order to clean the target surface, and stabilize the plasma. Then, the three samples of ZnO thin film were annealed at different temperatures which are 200°C, 300°C, and 400°C while one sample was acted as constant (as-deposited). The annealing process was carried out by using tube furnace for one hour. The annealed samples and as-deposited sample of ZnO thin film were characterized by using Filmetric, FTIR, and optical microscope in order to study the surface morphology, and optical properties of ZnO thin films.

3. RESULTS AND DISCUSSION

The thickness and refractive index of the ZnO thin films were determined by Filmetric F20 thin film analyzer and the reflectance spectrum over the wavenumber were analyzed. The value of

thickness, and refractive index of the samples were observed and recorded in Table 1 and the thickness of the thin films were increased as the thermal annealed temperatures were increased. However, at the temperature 400°C, the thickness of the thin film was decreased to 364.6 nm. The decreasing of the thin film's thickness was due to the evaporation of the organic and densification of the film [14].

Table 1: Thickness and Refractive Index of ZnO

Sample	Thickness, nm	Refractive Index
As-deposited	292.2	1.3365
Anneal at 200°C	218.3	1.6153
Anneal at 300°C	380.9	1.4154
Anneal at 400°C	364.6	1.3501

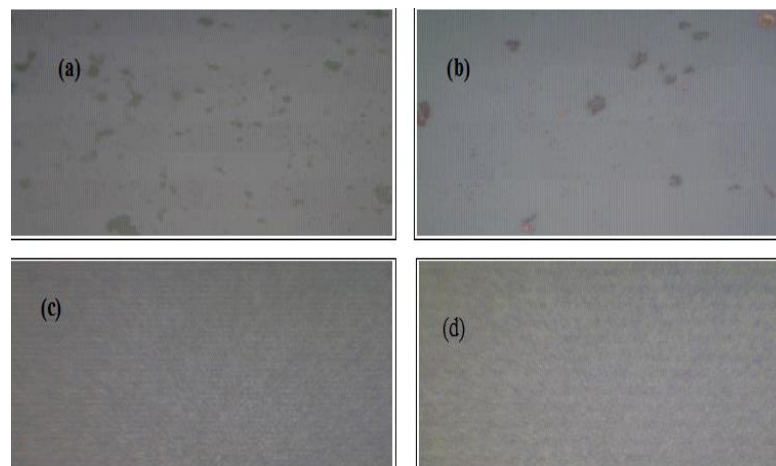


Figure 5: Optical Microscope of ZnO thin film: (a) as-deposited, (b) annealed at 200°C, (c) annealed at 300°C and (d) annealed at 400°C, respectively

For optical microscope analysis which is shown at Figure 5, at the low temperature of annealing process which is 200°C, the structure of the thin film is show the same morphology surface which is similar to the structure as-deposited ZnO. At as-deposited and anneal at 200°C, it were observed that a few small black holes were appeared in the samples. However, at the higher temperature of annealing which are 300°C and 400°C, the uniform film with grains are found to appear and the small holes were disappear after the thermal annealing above 200°C. The uniform grain that appear at high temperature of annealing is due to the agglomeration of the crystalline and the surface morphology of the sample is increased where the surface roughness of the samples were reduce which cause the surface of the sample become smoother.

4. CONCLUSION

The objectives of this research were to fabricate the ZnO thin film on the glass substrate by using RF sputtering, to anneal the ZnO thin film on the glass substrate at different temperature using thermal tube furnace and to characterize the annealed ZnO thin films on a glass substrate by using Filmetric, FTIR, and optical microscope. The optical properties and surface morphology of the As-deposited, and annealed ZnO thin film on glass substrate at 200°C, 300°C, and 400°C were analyzed. The FTIR analysis also shows that the higher temperature of annealing give a good transmittance which greater than 70% where it make the thin films have high transmittance

in the visible range. For the surface morphology, the optical microscope show that the ZnO thin film have increasing the surface roughness, uniform structure of grain and the surface of thin film become smoother as the annealed temperature increased at above 200°C.

ACKNOWLEDGEMENTS

This work has been supported by Faculty of Chemical Engineering of UiTM Pulau Pinang and Ministry of Higher Education, Malaysia

5. REFERENCES

- [1] S. J. Pearton, D. P. Norton, and K. Ip, "Recent progress in processing and properties of ZnO," vol. 50, pp. 293–340, 2005.
- [2] V. Khranovskyy and R. Yakimova, "Morphology engineering of ZnO nanostructures," no. 407, pp. 1533–1537, 2012.
- [3] L. L. Yang, *Synthesis and Characterization of ZnO Nanostructures*, no. 1327. 2010.
- [4] K. Lim, M. Azmi, A. Hamid, R. Shamsudin, I. Mansor, and W. Chiu, "Temperature-Driven Structural and Morphological Microstructures and Its Defect-Related Photoluminescence Properties," 2016.
- [5] J. M. Hancock and J. M. Hancock, "Formation and Analysis of Zinc Oxide Nanoparticles and Zinc Oxide Hexagonal Prisms and Optical Analysis of Cadmium Selenide Nanoparticles," 2013.
- [6] P. Kandasamy and A. Lourdasamy, "Studies on zinc oxide thin films by chemical spray pyrolysis technique," vol. 9, no. 11, pp. 261–266, 2014.
- [7] A. Raidou, M. Aggour, A. Qachaou, L. Laanab, and M. Fahoume, "Preparation And Characterisation Of Zno Thin Films Deposited By SILAR Method," vol. 12, no. 2, pp. 125–130, 2010.
- [8] M. A. Salim, "Effect of thickness on the optical properties of ZnO thin films prepared by pulsed laser deposition technique (PLD)," vol. 2, pp. 726–729, 2016.
- [9] P. Y. Dave, K. H. Patel, K. V Chauhan, A. Kumar, and S. K. Rawal, "“ Examination of zinc oxide films prepared by magnetron sputtering ,”" vol. 23, pp. 328–335, 2016.
- [10] Dedova and Tatjana, "Chemical Spray Pyrolysis Deposition of Zinc Sulfide Thin Films and Zinc Oxide Nanostructured Layers," 2007.
- [11] J. Husna, M. M. Aliyu, M. A. Islam, and P. Chelvanathan, "Influence of Annealing Temperature on the Properties of ZnO Thin Films Grown by Sputtering," vol. 25, pp. 55–61, 2012.
- [12] P. Hill, "Structure, Properties and Color," 2015.
- [13] E. S. Tuzemen, S. Elagoz, H. Sahin, K. Kara, R. Esen, and A. Bulut, "Effects of Annealing on Reflectance of ZnO Grown by PFCVAD," vol. 25, no. 2, pp. 41–50, 2013.

- [14]F. Xua, L., Li, X., Chen, Y. & Xu, “Structural and optical properties of ZnO thin films prepared by sol-gel method with different thickness,” *Appl. Surf. Sci.*, vol. 257, pp. 4031–4037, 2011.